공학박사 학위논문

Enhanced Oxidative Stability of Ether-based Solvents in Cross-linked Gel Electrolytes for 4V-class Lithium Metal Batteries

가교-젤 전해질내 에터 계열 용매의
산화안정성 향상을 통한 **4V**급 리튬금속전지 적용

2021년 8월

서울대학교 대학원
화학생물공학부
박 종 석

Enhanced Oxidative Stability of Ether-based Solvents in Cross-linked gel electrolytes for 4V-class Lithium Metal Batteries

가교-젤 전해질내 에터 계열 용매의
산화안정성 향상을 통한 4V급 리튬금속전지 적용
지도교수 최 장 욱

이 논문을 공학박사 학위논문으로 제출함

2021 년 7 월

서울대학교 대학원
화학생물공학부
박 종 석

박종석의 박사학위논문을 인준함
2021년 7 월

위 원 장	성 영 은
부 위 원 장	최 장 욱
위 원	이 규 태
위 원	김 기 재
위 원	조 용 남

Abstract

Enhanced Oxidative Stability of Ether-based Solvents in Cross-linked gel electrolytes for 4V-class Lithium Metal Batteries

Jongseok Park
School of Chemical and Biological Engineering
Seoul National University

As the concern for climate change and highly demanding requirement for energy supply emerges simultaneously, development of high energy density batteries to store electrical energy has come into an urgent technological issue. Since conventional Li-ion batteries with intercalation chemistry employing graphite and $LiCoO_2$ faced their limits in front of current highly demanding energy requirement stimulated by increasing EV market, various candidates for post Li-ion batteries are being challenged by battery researchers worldwide. Among them, Li metal batteries have drawn a sharp interest since the Li metal anode provides a lot higher specific capacity (3860 mAh g^{-1}) compared to commercial graphite anode (370 mAh g^{-1}). Due to its high theoretical specific capacity, lithium metal is highly expected to achieve the minimum target energy density of post Li-ion batteries (500 Wh/kg). However, due to highly

reducing nature of Li metal, uncontrolled interfacial reaction results in dendritic growth of Li metal, and subsequently, various problems such as safety hazard by short-circuiting, degraded energy density, and increased cell impedances. Consequently, various strategic approaches have been developed and Li metal batteries have been improved to some extent. By virtue of these enthusiastic challenges, Li metal polymer batteries have been even commercialized for electric vehicle applications by French Motor company, Bolloré. However, its features were far less than target energy density to become the real 'post Li-ion' and still it left challenging limitations to overcome.

Based on the serious limitations of previously commercialized Li metal polymer batteries, in this study, systematic design principles were constructed and employed comprehensively to develop high voltage lithium metal polymer batteries. 1) To resolve high cell impedance from low ionic conductivity of solid polymer electrolytes, liquid solvents (1,2-dimethoxyethane) was incorporated into the electrolyte. To retain the electrolyte to be compatible with Li metal, ether-based polymer and liquid solvents were utilized as in the Bolloré battery. 2) To compensate for the low anodic stability of ether based components, lithium salts were concentrated (~3.1M) and cross-linked polymeric matrix were employed to suppress diffusive flux of solvent molecules to reactive cathode surface, and consequently form robust inorganic-rich CEI layer for sustainable interfacial stability at cathode.

Three electrolytes were prepared and comparatively studied: Li salts in DME, DME with polyethylene oxide, and DME with cross-linked polyethylene oxide in same salt concentrations. Each electrolyte represents for liquid electrolyte, gel polymer electrolyte with linear polymer chains, and cross-linked gel polymer electrolyte. To prepare cross-linked gel electrolyte, ether-based triethylene glycol divinyl ether was employed as monomer to be in-situ polymerized by cationic initiator lithium difluoro-oxalatoborate (LiDFOB) salt. To prove initial hypothesis that diffusion of solvent molecules would be suppressed in cross-linked polymeric matrix, pulsed-field gradient NMR (PFG-NMR) spectroscopic analysis was conducted for liquid and gel polymer electrolytes to evaluate diffusive motion of solvents in each electrolyte. As expected, diffusion of solvent molecules was highly suppressed in cross-linked polymeric matrix compared to that in liquid and linear chain gel polymer electrolyte. Additionally, not only solvent molecules, but also linear polymer chains were found to diffuse in corresponding gel electrolyte while the absence of polymer diffusion in cross-linked gel electrolyte was revealed by PFG-NMR analysis.

To confirm the correlation between diffusion of solvent molecules and electrochemical performances, Li|NCM cells with liquid and gel electrolytes were tested under constant current charge/discharge. Regardless of salt concentration, cyclic stability of Li|NCM cell was the highest with cross-linked gel electrolytes. Through the respective analyses of cathode and anode after

Li|NCM charge/discharge cycling tests, different interfacial phenomena were induced by each electrolyte. Due to suppressed diffusion of solvent molecules in cross-linked gel electrolyte, anions contribute dominantly to the formation of robust inorganic-rich CEI layer to enhance oxidative stability of electrolyte. In the Li metal anode side, mechanically suppressed dendrite growth by cross-linked gel electrolyte contributes to stable electrochemical performance rather than chemical advantages. Finally, it was confirmed that design principles constructed and utilized in this study, worked properly as evidenced by various spectroscopic and interface analyses.

Keywords: lithium metal battery, gel polymer electrolyte, energy storage system, pulsed-field nuclear magnetic resonance, in-situ polymerization, cathode-electrolyte interphase layer

Student number: 2015-21021

Table of Contents

List of Tables

List of Figures

1. Introduction

1.1 Beyond Li-ion: Lithium metal batteries

The basis of energy supply is rapidly transforming from carbonaceous fossil-fuel based convention into electricity-based platform due to simultaneous explosion of energy demand and concern for carbon-derived global warming. The two most important prerequisite for electricity based energy platform is 1) generation of electricity from renewable resources, and 2) storage of electrical energy for stable and delicate response to high fluctuation of energy consuming rate. To date, rechargeable batteries, especially Li-ion batteries (LIBs), have been successfully commercialized as electrical energy platform predominantly for lab-tops, smartphones and household appliances during the past decades.[1]

Conventional LIBs are based on intercalation chemistry of Li cations, employing graphite anode and $LiCoO_2$ cathode which are both in layered crystal structure providing interlayer spaces to accommodate Li. Recently, Silicon-based alloying anodes and $LiNi_xCo_yMn_{1-x-y}$ (NCM) layered cathodes are rapidly replacing conventional electrodes due to their higher theoretical energy density to meet the sudden boost in energy requirements, especially triggered by electric vehicles (EVs). However, this current-emerged highly demanding quantitative and environmental requirements for energy supply are not possible to be satisfied enough with current lithium-ion batteries in spite of the considerable advance in Si- and NCM-based electrodes. Accordingly,

batteries beyond the intercalation chemistry should be employed to meet challenging level of energy demand and realize complete transformation of energy platform into electricity-based one.

In this respect, diverse candidates have emerged as post Li-ion battery (post-LIB) technologies. Among them, Li metal batteries have drawn a sharp interest since the Li metal anode provides a lot higher specific capacity (3860 mAh g^{-1}) compared to commercial graphite anode (370 mAh g^{-1}). Due to its high theoretical specific capacity, lithium metal is highly expected to achieve the widely recognized target energy density (450~500Wh/kg, **Table 1-1**).[2]

However, the Li metal anode is highly reactive against aprotic organic solvents which are widely used in the electrolytes of current LIBs. This highly reactive surface of lithium metal undergoes interfacial reaction with aprotic organic liquid electrolytes, forming solid-electrolyte interphase (SEI) layer which is insulating enough to prevent further reaction consuming both electrolyte components and lithium metal. The SEI layer, without any sophisticated treatment, becomes non-uniform with random spatial distribution in thickness, chemical composition, ionic conductivity and porosity. The non-uniformity of SEI layer results in spatially different energy barrier for electrodeposition, consequently allowing high spatial dependence during electrodeposition of lithium through it. This non-uniform and uncontrolled interfacial reaction deteriorates upon electrochemical charge/discharge cycling. Therefore, enabling the interfacial reactions controllable and uniform becomes

the key challenge to commercialize lithium metal batteries in a genuine manner.

1.2 Non-uniform SEI & Dendrites

Most of adverse phenomena that hinder stable electrochemical cycling of lithium are rooted in spatially non-uniform SEI layer.[3] This results in site-dependent energy barrier for electrochemical plating of Li. Consequently, there appears higher growth rate at locally preferred site with low energy barrier for electrochemical plating. Relative high growth rate on a specific site increases roughness of surface morphology, and relative elevation in growth rate, especially at protruded area, becomes aggravated. Upon charge/discharge (electrochemical plating/stripping of Li) cycling, initially protruded morphology becomes spiny due to deteriorated difference in growth rate. This spine form of lithium, so-called *Dendrites*, construct the axis of evil against the development of lithium metal batteries.[3b, 4]

The uncontrolled growth of dendrites delivers three major damage to electrochemical properties of lithium metal batteries. 1) Safety: Continuous growth of dendrites can penetrate into tortuous pore structure of separator and induce short-circuit of cell. In this case, large electrical current can intensively pass through the dendritic short-circuit path, incurring thermal runaway and serious safety hazard. 2) Degradation of energy density: As-formed dendrites can break the SEI layer, exposing fresh lithium. Since lithium is highly reactive

against most organic electrolytes, SEI layer immediately forms on the exposed interface. Fresh lithium is ceaselessly exposed to the electrolyte due to breakage of SEI layer by dendrites, consuming both electrolyte components and lithium anode. In addition, repeated plating/stripping of Li partially makes lost connection with the bulk electrode and electrochemically inactive. As these inactive pieces of lithium become accumulated, initially supplied amount of lithium cannot be fully utilized after prolonged cycling, and coulombic efficiency degrades. 3) Increase in cell impedance: as electrically disconnected inactive lithium becomes piled up, porous inactive layer forms on the electrode. This porous layer extends the pathway of ions to active electrode by increasing tortuosity, therefore causing decreased ionic conductivity and increased cell impedance.

To overcome these issues of non-uniform SEI and dendrites, diverse novel approach has been developed and made significant advances in lithium metal batteries.

1.3 Current challenges for uniform electroplating of Li

Since the requirement for high-energy-density batteries has been triggered by emerging trend of EV, intense efforts have been made by global researchers as indicated by sudden rise in the number of research papers on lithium metal batteries.[5] Among 17,376 research papers published since 1976, more than

10,000 of those have been published after 2015. These enthusiastic interests on lithium metal batteries, as is indicated by the number of research papers, have produced diverse novel approaches to make significant advances in the development of lithium metal batteries. These can be summarized into 3 categories and would be introduced in this chapter.

1.3.1 *3D conductive hosts to accommodate electrodeposited Li*

During the initial nucleation of electrodeposition, it is unavoidable to make surface morphology without roughness and protruded area. Then, electric field focus on these sharpened area, allowing further localized growth and make dendrites. This phenomenon deteriorates more seriously under high current density (> 4mA cm^{-2}).

3D conductive hosts composed of carbonaceous or metallic materials in porous structure provide high surface-to-volume ratio, alleviating effective current density compared to pristine flat current collectors (e.g. Cu foil) under same charge/discharge conditions. Therefore, dendrite growth also can be alleviated under relatively lower current density.

Cui et al. designed porous films with stacked reduced graphene oxide (rGO) and infiltrated molten lithium in the host.[6] The rGO film has high electrical conductivity and surface-to-volume ratio, significantly reduced effective current density. Consequently, this designed anode host suppressed dendrite growth and the rate of consumption of active components such as

lithium and electrolyte.

Choi et al. designed highly elastic binders to enhance the durability of functionalized CNT-based 3D conductive host.[7] They utilized polyrotaxane-polyacrylic acid (PR-PAA) binder to enable CNT host adaptively respond to huge dynamic volume change during lithium plating/stripping. By virtue of high elasticity of PR-PAA binder, CNT host could represent enhanced cyclic stability compared to CNT hosts with polyvinyl alcohol (PVA) binder or without polymer binder.

Yu et al. employed Cu nanowires to construct 3D conductive host.[8] They designed free-standing Cu nanowire network current collector to accommodate the Li metal inside the porous nanostructure to limit the growth of Li dendrite and enhanced the cycling stability of the Li metal anode.

Besides, various carbonaceous or metallic conductive hosts were strategically designed.[9] They made substantial advancements in dendrite-free electroplating. However, it is unavoidable to offset the volumetric energy decrease due to the excess volume of host itself to accommodate sufficient amount of lithium.

1.3.2 *Protective film and artificial SEI layer*

Dendrite growth during electrodeposition of lithium can be suppressed both mechanically (applied pressure) and chemically (stable SEI components) by rationally designed protective films or artificial SEI layers. A layer that can

provide shear modulus of ~1 GPa can partly suppress Li dendrites.[3b] However, pristine SEI layers always exhibits lower and spatially heterogeneous shear modulus. Artificial films can resolve these issues by providing uniform and high enough mechanical properties.

For this kind of perspective approach, Cui et al. employed commercially available "Silly Putty" as a coating layer to electroplate lithium in homogeneous morphology by virtue of adaptive and dynamic mechanical property.[10] "Silly Putty" has siloxane-based polymer chains and borate-based cross-linkers. This cross-linker can dynamically exchange bonding sites on polymer chain so that provide dynamic mechanical modulus depending on shear rate. The higher the shear rate, the stiffer the polymer becomes. Under high current electroplating, growing dendrites at high rate are more suppressed with higher mechanical modulus due to adaptive mechanical property of "Silly Putty" coating layer.

Wang et al. adopted a strategy and designed a protective layer that chemically homogenize electrodeposition of lithium.[11] They synthesized a polymer in which rationally chosen functional groups are incorporated. 1,3-Dioxolane and fluorosulfonyl (FSI) are renowned compounds that induce stable deposition morphology acting within the SEI layer. Wang's group synthesized a copolymer from two vinyl monomers having 1,3-dioxolane and FSI group, respectively. Finally, composite protective film with graphene oxide added, they demonstrated a Li|NCM cell with long-term cyclic stability under lean

electrolyte condition (~7μL mAh^{-1}).

Comprehensive approach has been taken by Helms et al., providing design principles for dendrite suppression from both mechanical and chemical perspective.[12] They set two parameters, partial molar volume of Li^+ (V_{Li+}) and shear modulus, to evaluate the degree of dendrite growth. With some DFT results, they recognized two different regimes of pressure-driven dendrite blocking and chemical driven dendrite suppression. Finally, they designed polymeric coating in which highly concentrated tetrabutyl ammonium fluoride (TBAF) are incorporated to generate LiF after electrolyte infiltration. This coating layer belongs to soft-highly concentrated dendrite suppression regime and achieved stable electrochemical cycling of Li|NCM (~1.44mAh cm^{-2}, N/P = 5) cells over 300 cycles.

Although artificial protective films have made a substantial advance for the operation of lithium metal batteries, still it offsets the energy density. In addition, there is always a limitation in the durability of mechanical property and sustainable supply of chemically stable SEI components with a limited amount of incorporated artificial film.

1.3.3 *Electrolyte modification and solid electrolytes*

SEI forms when lithium metal contacts with electrolyte. Therefore, almost limitless number of strategies can be found in electrolyte modification. The main purpose of electrolyte modification is to design SEI layer *in operando*.

One of major criteria to stabilize SEI layer is how rich polymeric or inorganic components are incorporated in it which are not dissolved into organic electrolytes once formed.

Researchers developed various types of electrolytes to enrich insoluble (mainly inorganic) components in the SEI layer. To give inorganic-rich SEI, interfacial reaction of anions in lithium salts should be predominated over organic solvents or other components during electrochemical charge/discharge. For this purpose, the number of anions in solvation sheath surrounding Li^+ should be increased for them to participate in the interfacial reaction.

One of direct intuitional strategy for this is increasing salt concentration to almost solubility limit.[13] Solvation structure varies compared to conventional dilute (~1M) electrolytes, and also the portion of anions in solvation sheath is significantly higher. Numerous reports demonstrate stabilized operation of lithium metal batteries with various concentrated electrolytes and post-mortem analyses revealing enriched inorganic components in respective SEI layers.

Another effective strategy has been developed recently with organic solvents having low solvating ability, diluent solvents.[14] When added into electrolytes, diluents barely interact with ions in the electrolytes although they are homogeneously mixed with electrolytes. By virtue of these diluents, conventional organic solvents can exceptionally interact with Li^+ and

experience locally concentrated atmosphere (locally highly concentrated electrolytes, LHCE). Consequently, anions in solvation sheath becomes more influential even though bulk concentration of the electrolyte is similar to those of conventional electrolytes and anions contributes dominantly in the formation of SEI layer.

The extreme case to grant solid-insoluble interfacial component on lithium metal anode is the *solid electrolyte*.[15] Solid electrolytes can be divided into two categories: inorganic solid electrolytes (oxide-based and sulfide-based) and solid polymer electrolytes. Both types of solid electrolytes provide highest safety performance (fire retardant) among various organic liquid electrolyte systems. In addition, these are recognized to effectively suppress dendrite growth mainly by mechanical strength. However, this robustness instead deteriorates interfacial contact. In case of sulfide-based inorganic electrolytes, additionally, it is not compatible with lithium metal electrode because of serious unfavorable side-reactions at the interface. On the other hand, oxide-based inorganic and solid-polymer electrolytes suffer from intrinsically low ionic conductivity. Despite of these major drawbacks, battery researchers persistently endeavor to modify and utilize solid electrolytes for intrinsic safety performance of extremely low flammability.

1.4 Lessons from commercialized lithium metal batteries

Among various strategic approaches introduced above, one representative case that has once been commercialized is lithium metal-polymer batteries. Bolloré groups launched an electric vehicle, Bluecar®, equipped with a 30 kWh lithium-polymer battery (LMP) to guarantee a driving range of 250 km and a maximum speed of 120 km h^{-1}.[15e] This LMP battery in Bluecar® is comprised of LiTFSI/polyethylene oxide (PEO)-based polymer electrolyte, $LiFePO_4$ cathode, and Li metal anode.[15c] Until 2015, the safety record for Bolloré's batteries is outstanding, indicated by no safety-related issue in Indianapolis, nor in Paris with 3,000 cars in service and accumulated 10 million driven miles.[16] However, Bolloré's batteries are not quite ready for mass-market application because these need to be warmed up (>80°C) prior to power the car. 250 km of driving range is either not sufficient to meet the currently required energy density.[2b]

These limitations in the electrochemical performance of LMP battery is originated from intrinsically low ionic conductivity of solid PEO electrolytes. Further enhancement of energy density by utilizing high voltage cathode (e.g. NCM cathodes) rather than LFP is also limited due to low anodic stability of PEO electrolyte (<4V).[17] Inevitable incorporation of polymers and salts into cathode to percolate the ionic conductive pathway further decrease the energy density of LMP battery. Consequently, comprehensive design of polymer-based electrolyte is highly required for further enhancement of lithium metal

batteries without any counteraction to the intrinsic safety performance of polymer electrolytes.

1.5 Design principles of this study: comprehensive approach for lithium metal batteries

A Comprehensive strategic approach is suggested in this study with point by point address to the limitations in existing PEO-based solid polymer electrolytes.

To increase the ionic conductivity, a portion of organic liquid solvent was included in designed electrolyte system (Gel polymer electrolyte, GPE). 1,2-Dimethoxyethane (DME) was chosen as liquid solvent for this system, considering the relative stability against lithium metal anode compared to carbonate counterparts.[18] Since increasing liquid content deters mechanical strength of the electrolyte, additional modifications were applied to PEO-based polymer matrix rather than simple inconsiderate incorporation of liquid. Instead of PEO in long and linear molecular chain structure, an ethylene oxide-based cross-linkable monomer, triethylene glycol divinyl ether (TEGDVE), was chosen to compensate for liquid-induced reduction of mechanical strength by cross-linked polymer matrix. In addition, TEGDVE monomer can be in-situ polymerized thermally (~60°C) after being injected into the cell in originally liquid state. The in-situ formed polymeric matrix can form interfacial contact

with lithium metal anode and corresponding cathode in a more conformal structure than pure solid electrolytes which form point contact at the interface.

To enhance the poor anodic stability of PEO, salt concentration is increased to moderate degree (~3M). Besides, TEGDVE-derived cross-linked matrix can also function at the interface with high voltage cathode. As is well known, cathode electrolyte interphase (CEI) layer forms at the interface between electrolyte and cathode particles, modification of CEI layer can have significant influence on the anodic stability.[19] Since cross-linked matrix can physically block the diffusion rate of liquid solvent molecules, anions predominantly participate in the formation of CEI layer during the first charging step. Then, the preformed inorganic-rich robust CEI layer enlarge the anodic stability continuously during the subsequent charge/discharge cycling.

Moreover, it is possible to get rid of previously indispensable incorporation of polymers and salts into cathode to let ion conduction percolate by the in-situ polymerization of TEGDVE. It is because TEGDVE-based gel electrolytes can penetrate into pores of conventionally fabricated cathodes as in liquid precursor and can be polymerized afterward. In addition, by virtue of this in-situ polymerization, combination with another strategy for lithium metal anode is possible. For example, in-situ formed polymeric matrix can be combined with 3D conductive host since it can be infiltrated into and sufficiently wet 3D porous host structure as originally a liquid precursor state prior to solidification.[20]

These respective solutions to the limitations of previous lithium metal polymer batteries would be further introduced in detail in the following chapters.

Parameter at cell level	**Unit**	**Condition**	**Target (~2030)**
Specific energy	Wh/kg	@ 1/3C charge and discharge at 25℃ (charging with CC and CV step)	**450**
Energy density	Wh/l		**1000**
Continuous specific energy	W/kg	180s, SOC100%-10%, 25℃	**1000**
Continuous energy density	W/l		**2200**
Charging rate	C(1/h)	SOC 0%-80%	**3**
Self-discharge	%	SOC100%, 25℃, 30 days	**1**
Cost	€/kWh		**220**

Table 1. Battery requirements for future battery electric vehicle (BEV) applications. Adapted from EUCAR.[2b]

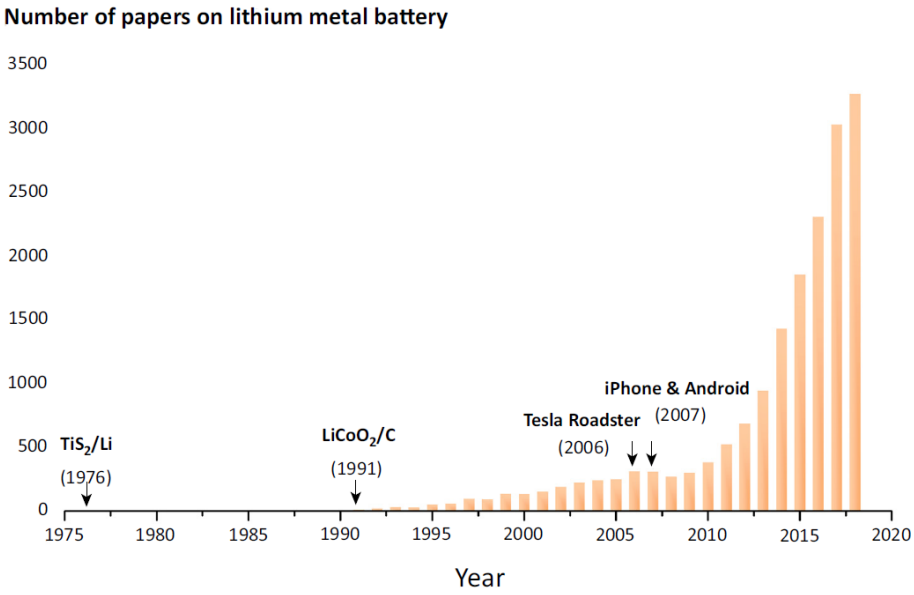

Figure 1-1. The number of research papers on lithium metal battery published from 1976 to 2018. Adapted from Meng et al.[5]

Strategy	Method	Reference
3D conductive Li host	rGO + molten Li	[6]
	CNT + elastic binder	[7a]
	Cu nanowire composite	[8]
Protective layer (Artificial SEI)	Siloxane polymer + borate cross-linker (dynamic cross-linking)	[10]
	Vinyl FSI + Vinyl DOL + rGO composite film	[11]
	Polyimide + TBAF (cation metathesis)	[12]
Modified electrolyte	Concentrated electrolytes	[13]
	Locally highly concentrated electrolytes with fluorinated diluents	[14]
	Solid electrolytes	[15]

Table 2. Current challenges for uniform and stable electroplating of Li metal anodes.

Motor/Battery	Parameter	Unit	Value
Motor	Horsepower	kW	**30, 50(max)**
	Max. torque	Nm	**170**
Battery	Power	kWh	**28**
	Weight	kg	**240**
	Recharging time to 100%	hrs	**4**
	Minimum/Maximum Battery Voltage	V	**243/374**
	Internal temperature	^{o}C	**90**
	Operating temperature	^{o}C	**-20 ~ 60**

Table 3. Motor/Battery features of Bolloré Bluecar.

2. Design of gel polymer electrolyte for high-voltage lithium metal batteries

2.1 Electrolyte design for enhanced oxidation stability

To resolve low ionic conductivity and oxidation stability of PEO-based LMP battery, several design principles have been applied. To increase the ionic conductivity, a portion of organic liquid solvent, 1,2-dimethoxyethane (DME) was included with polymer components to form a gel-polymer electrolyte. Subsequently, to enhance the poor anodic stability of this PEO-based gel-polymer electrolyte, two additional strategies were employed. First, salt concentration was increased to moderate degree (~3M). Lastly, PEO-based polymer matrix was modified into cross-linked structure by using in-situ polymerization of divinyl monomer, triethylene glycol divinyl ether (TEGDVE).

Cross-linked polymer matrix can modify cathode-electrolyte interphase (CEI) layer by tuning the degree of participation of electrolyte components to the interfacial reaction. In the open-circuit state, electrolyte components can contact to surfaces of cathode particles only by diffusion both for solvent and ions. However, during the initial charge (initial formation of CEI layer), ion motions are predominantly determined by migration due to strong electric field under charging condition while motion of solvent molecules is determined mainly by diffusion as same for open-circuit state.

During the initial charging, anions migrate and solvent molecules diffuse to cathode surface and participate in the CEI formation. Therefore, if a polymeric matrix that can physically block the diffusion of solvent molecules to electrode, the interfacial reaction at cathode can be dominated by contribution of anions forming inorganic-rich CEI layer. The robust inorganic-rich CEI layer can protect electrolytes from oxidative decomposition during subsequent electrochemical cycling. This phenomenon is illustrated in **Figure 2-1**. In the following chapters, anion-derived cathode electrolyte interphase by confinement effect of solvents in cross-linked gel polymer electrolyte would be introduced by comparative analyses of three electrolyte samples.

2.2 Experimental

2.2.1 *Experiments for comparative study*

Three electrolyte samples were prepared for comparative study to prove the confinement of solvents in cross-linked polymer matrix. Lithium salts (LiTFSI and LiDFOB), 1,2-dimethoxyethane (DME), triethylene glycol divinyl ether (TEGDVE), and polyethylene oxide (PEO, M_w ~100,000) were used as purchased from Sigma-aldrich. Li metal foils (150μm thick for LSV and chronoamperometry, and 40μm thick for full cell cycling), NCM622 powders, and super-P were purchased from Wellcos corporation. Kynar PVDF (Mw ~ 534,000) was purchased from Sigma-aldrich. 3.1M LiTFSI salt was dissolved

in liquid DME, DME with 20wt% PEO (Mw 100,000 g mol^{-1}), and DME with 20wt% TEGDVE. For in-situ polymerization (cross-linking) of TEGDVE 10wt% of LiDFOB in DME solution was added to respective electrolytes. These electrolytes are hereafter named 3.1M DME, 3.1M PEO20, and 3.1M CPE20 (cross-linked polymer electrolyte), respectively. These three electrolyte represent for electrolyte without polymer matrix (3.1M DME), gel electrolyte with linear polymer chains (3.1M PEO20), and gel electrolyte with cross-linked polymer matrix (3.1M CPE20). To prove suppression of solvent diffusion according to the structure of polymeric matrix, electrolytes with lower concentration were prepared by the same experimental procedure (2.0M DME, 2.0M PEO20, and 2.0M CPE20, respectively).

2.2.2 *Characterization*

The molecular structuring in liquid and gel polymer electrolytes were studied using attenuated total reflectance − Fourier transform infrared spectroscopy (ATR-FTIR) on a TENSOR27 FTIR spectrometer (Bruker, Germany) equipped with a deuterated L-alanine doped triglycene sulphate (DLATGS) detector and a single reflection diamond ATR accessory. Pulsed-field-gradient nuclear magnetic resonance (PFG-NMR) measurements were performed using a Bruker Avance III HD spectrometer with an UltraShield™ 500 MHz superconducting magnet equipped with a 5mm Diff30 pulsed field gradient probe and current amplifier to study the self-diffusion coefficients of DME

molecules in each liquid and gel polymer electrolytes. The Raman spectra of various electrolytes were recorded using a Raman spectrometer (DXR2xi, Thermo Fisher, USA). SEM images of lithium metal surfaces after electrochemical cycling with various liquid and gel polymer electrolytes were obtained using a field-emission scanning electron microscope operating at 2 kV with an in-lens detector (SUPRA 55VP, Carl Zeiss). Isothermal thermogravimetric analysis (TGA) was conducted using digital electronic scale by measuring relative weight compared to initial states of each liquid and gel polymer electrolytes (2.0 M) in open space at 80°C. The chemical nature of the SEI layers on Li and CEI layers on cathode particles were investigated using XPS (AXIS SUPRA, Kratos, U.K.) with Al-Kα radiation (1486.6 eV) for the X-ray source. The XPS spectra were calibrated by aligning the C 1s peak at 284.6 eV.

2.2.3 *Electrochemical tests*

All battery components used in this work were commercially available and all electrochemical tests were carried out in a 2032-type coin-cell configuration. All cells were fabricated in an argon-filled glovebox, and one layer of Celgard 2400 or 3501 was used as a separator. Linear sweep voltammetry was carried out on a Wonatech ZIVE SP2 system.

The cycling tests for coin cells were carried out on an WBCS3000 (Wonatech) instrument. The anodic LSV tests were over a voltage range of 2.5 to 7 V with

Al-deposited stainless steel as a counter electrode and Li metal as a reference electrode. The Li|NMC full cells were cycled with the following method: the cells were cycled for two activation cycles at constant current density of C/10 charge/discharge, followed by charge/discharge cycles at different rates (C/3 discharge, C/3 charge for 2.0M electrolytes and C/3 charge, C/2 discharge for 3.1M electrolytes) between 3.0V and 4.2V. All cells were cycled under high temperature condition (60°C). Chronoamperometry tests were conducted with Li|NCM full cells measuring current density for 24 hours (or 6 hours) at fixed potentials of 4.2V, 4.3V, 4.4V, and 4.5V for 3.1 M electrolytes and 4.0V, 4.1V, 4.2V and 4.3V for 2.0 M electrolytes. Initial charging to 4.2V (or 4.0V) was reached under constant current at C/10, followed by stepwise increase to higher potentials, subsequently. NCM622 electrodes were fabricated by blade-casting the electrode slurry made of dispersed NCM622 particles, PVDF binder, and super-P additive at 95:2.5:2.5 ratio in NMP solvent. The mass loading of NCM622 was ~2.4 mAh cm^{-2} for all the electrochemical tests if used. Li|Li symmetric cells were fabricated with thin film Li metals (~40 μm) into CR2032 type coin cells with respective electrolytes under constant current charge/discharge.

2.3 Results and discussion

2.3.1 *Formation of in-situ cross-linked polymer matrix*

Preparation of 3.1 M DME and PEO20 electrolytes were conducted by simple mixing of each required components. For 3.1M CPE20, in-situ thermal polymerization was required to internally form web-like cross-linked polymeric matrix. The schematic illustration was represented in **Figure 2-2**. The precursor solution made of only TEGDVE monomer, DME solvent, and LiTFSI salts were prepared by simple mixing, followed by adding initiator solution composed of LiDFOB/DME. After aging at moderate high temperature (60°C) for 6 hours, in-situ polymerization of TEGDVE monomers were completed by cationic polymerization of vinyl groups by Lewis acidic borate salts as shown in **Figure 2-3**.[21] By FT-IR analysis, it is confirmed that active carbon double bonds (~1660 cm^{-1}) were inactivated to IR since vinyl groups in TEGDVE are transformed into single carbon bonds after aging at 60°C (**Figure 2-4, a**).[22] The FT-IR spectra indicate complete polymerization of TEGDVE monomers, thermally. In addition, the higher the salt concentration, the lower the intensity of C-O stretching (~1100 cm^{-1}) was found in IR spectra due to strong coordination of DME to Li^{+} as concentration becomes higher. The transparent gel polymer electrolytes with cross-linked TEGDVE matrix indicates the absence of optical anisotropy in corresponding gel and amorphous nature in molecular structure (**Figure 2-4, b**).

2.3.2 *Enhanced anodic stability with cross-linked polymer matrix*

To elucidate the correlation between solvation structure in each electrolytes and anodic stability, Raman spectroscopic analyses were conducted for each samples. As shown in Raman spectra in **Figure 2-5**, solvation structures were compared according to varying salt concentrations in liquid electrolytes (1.0, 2.0 and 3.1M). In 1.0 M DME electrolyte, both Raman active Li-O interaction (~875 cm^{-1}) and C-O stretching bonds (~850 cm^{-1}) are found in high intensity while C-O stretching becomes almost absent due to complete coordination of DME to Li^+ leaving no free solvent molecules.[23] Anions in solvation structure behaves accordingly to the salt concentration. Raman active TFSI- anions are found as fully dissociated free state (solvent-separated ion pairs, ~ 737 cm^{-1}) in lower concentrations (1.0 and 2.0 M), while anions exist as associated ion pairs with Li^+ (Li-TFSI, ~740 cm^{-1}) at high concentration (3.1M) due to high Li^+/solvent molar ratio, consequently lower coordination number of solvents to Li^+.[24] In addition, it is confirmed that solvation structures of three electrolyte samples (3.1M DME, PEO20 and CPE20, each with different polymer contents and structure of polymeric matrix) are similar because of the equal salt concentration, consequently similar coordination number of solvents to Li^+. These have similar peak positions for associated anions (~740 cm^{-1}) and similar intensities in strong Li-O and weak C-O interaction (875 and 850 cm^{-1}, respectively).

Followed by spectroscopic analyses of solvation structures in each

electrolyte, linear sweep voltammetry tests were conducted for above mentioned electrolytes to figure out the correlation between solvation structure and anodic stability (**Figure 2-6**). As the salt concentration increases, anodic potential stability limit is increased accordingly. Explosive electrical currents induced by oxidative decomposition of electrolytes at potentials over stability limit flow after 4.5V in Li|Al cell with 1.0M DME, 4.75V with 2.0M DME, and 6.0V with 3.1M DME. At fixed concentration (3.1M), no significant difference in anodic stability was detected by linear sweep voltammetry between electrolytes with polymers of different kinds.

For detailed analysis on anodic stability of electrolytes, chronoamperometry tests were conducted for 3.1M DME, PEO20 and CPE20 electrolytes in Li|NCM coin cells (**Figure 2-7**). During chronoamperometry tests, current density is recorded at fixed potentials after stepwise increase. After a few hours of complete charging process, diminutive leakage currents continuously occur due to faradaic reactions such as oxidative decomposition of electrolytes by charged NCM particles other than Li^+ intercalation.[25] The more stable the electrolyte, the lower the leakage current is.[26] Therefore, it is possible to correlate the measured electrical currents by chronoamperometry tests with oxidative stability against charged NCM particles. In addition, anodic stability against NCM particles provides more practical information about target electrolyte. While anodic currents were similar in LSV tests, anodic currents by chronoamperometry were significantly different for each liquid and

gel polymer electrolyte as shown in **Figure 2-7**. At 4.5V, high and rapid increasing leakage current was measured with 3.1M DME electrolyte, indicating unstable behavior against oxidative environment. However, relatively stable and slow increase in leakage current was measured with 3.1M CPE20 electrolyte and leakage current occurred at intermediate degree with 3.1M PEO20 electrolyte. This difference in anodic leakage currents imply polymeric matrix, especially cross-linked polymeric matrix, can further provide enhanced oxidation stability. Since the main component experience oxidative decomposition is solvents under high voltage, it is hypothesized that diffusive solvent flux into cathode particles are suppressed by polymeric matrices in various conformation. This hypothesis was proved by further analysis by 1H PFG-NMR and the results are discussed in following chapters.

2.3.3 *Physically suppressed diffusion in cross-linked polymer matrix*

Diffusion coefficients of individual components in a mixture can be measured by pulsed-field-gradient NMR spectroscopy (PFG-NMR).[27] During the analysis procedure of PFG-NMR, conventional NMR spectra is obtained, followed by measurement of diffusion coefficients at each peak obtained ahead. As shown in **Figure 2-8**, for example, 1,2-dimethoxyethane has two 1H peaks at chemical shift of ~3.5 and 3.8 ppm.[28] With PFG-NMR analysis, diffusion coefficients of these hydrogens in a certain mixture are obtained and can be demonstrated in 3D or contour 2D mapping.[29] Since these hydrogens are in a

same molecule, highly similar diffusion coefficients are necessarily recorded. In this study, consequently, diffusive behaviors of DME molecules in various electrolytes can be observed by PFG-NMR analysis.

Accordingly, PFG-NMR contour spectra of 3.1M DME, PEO20 and CPE20 electrolytes are represented in **Figure 2-9**. Since there are no other organic components showing peaks at chemical shifts between 3.5 ~ 4.0 ppm, it can be confirmed that only DME molecules can be assigned to these peaks. The diffusion coefficients of DME were 5.64, 3.52 and 3.70 x 10^{-10} m^2 s^{-1}, for 3.1M DME, PEO20, and CPE20 electrolytes, respectively. As is expected, the rate of diffusion in electrolytes with polymeric matrices was suppressed by ~40% compared to that in liquid electrolyte. This can be a critical evidence of above mentioned hypothesis that highly alleviated oxidative decomposition of electrolyte is originated from suppressed diffusive flux of solvents to reactive cathode surfaces.[30]

2.3.4 *Further proof of suppressed diffusion with electrolytes in lower concentration*

To provide more solid and thorough evidence for suppressed diffusive flux of solvents in electrolytes with polymeric matrices, PFG-NMR analyses for electrolytes in lower concentrations were conducted (2.0M DME, PEO20 and CPE20).[27] Preparation of these electrolytes were conducted following the same procedure as for 3.1M electrolytes, except for salt contents. As shown in

Figure 2-11, the diffusion coefficients of DME were 6.44, 0.597 and 0.6 x 10^{-9} m^2 s^{-1}, for 2.0M DME, PEO20, and CPE20 electrolytes, respectively. As is expected, the rate of diffusion in electrolytes with polymeric matrices was relatively suppressed while the difference was significantly enlarged compared to concentrated electrolytes (over an order of magnitude lowered).

Diffusion coefficient implies how mobile a specific component is. Thus, if diffusive behavior of liquid is inhibited by a certain degree, it can be reflected in the rate of evaporation at the open surface of a material. Since diffusion coefficients of DME molecules in respective 2.0M electrolytes were different, the rate of evaporation at the surfaces of each electrolyte would also be different. The rate of evaporation of DME molecules in each electrolyte at 80°C were evaluated by isothermal TGA and shown in **Figure 2-12**. Initial 1.2g of each electrolyte was put into a 10ml open vial, and aged at 80°C. During the aging process, mass of each electrolyte was measured at every 1-minute time interval. Time required to reach 70% of initial mass was 50, 150 and 240 min for 2.0M DME, PEO20 and CPE20, respectively. Evaporation of DME was much slower in electrolytes with polymeric matrices due to physically suppressed free motion of DME molecules. This can be an additional critical evidence to prove that polymer contents can reduce the diffusive flux of solvents to reactive cathode surfaces, and consequently enhancing anodic stability of corresponding electrolyte.

Accordingly, anodic stability of 2.0M CPE20 is much higher than

DME and PEO20 as shown in electrochemical profiles of chronoamperometry tests for respective electrolytes (**Figure 2-10**). Therefore, it can be concluded that, regardless of salt concentration, polymeric matrices can decrease diffusive flux of liquid molecules to reactive surface of cathode particles and protect those from oxidative decomposition. However, there exists a point to debate for what reason CPE20 electrolytes are higher in anodic stability although diffusion coefficients of DME molecules in those are slightly higher. This seemingly contradictory problem can be resolved by further observation of PFG-NMR spectra with another focus on the diffusive behavior of polymer chains in each gel polymer electrolyte with linear PEO chains or cross-linked TEGDVE matrix.

2.3.5 *Diffusion of polymer chains in electrolyte with different polymer structure*

Although diffusion coefficients of DME molecules in PEO20 and CPE20 are almost indifferent, respective polymer components (linear PEO chains and cross-linked TEGDVE matrix) behave distinctively. The critical phenomenological difference comes from diffusion of polymer chains. As shown in **Figure 2-13**, the representative NMR peak of hydrogens in PEO chains appears at ~3.95 ppm indicating PEO chains diffuse both in 2.0M and 3.1M PEO20 electrolytes (with diffusion coefficients of 2.40 and 4.17 x 10^{-10} m^2 s^{-1}, respectively). The higher diffusion coefficient of DME in 3.1M PEO20

compared to that in 2.0M PEO20 indicates the effect of plasticized and liberated state of PEO chains by concentrated LiTFSI salt.

Contrarily, the absence of polymer diffusion in 2.0M and 3.1M CPE20 electrolytes was indicated by magnified observation of PFG-NMR contour plot shown in **Figure 2-14**. This implies that diffusive polymers in PEO20 can further increase the flux of organic components heading for oxidizing NCM surface, resultantly increasing the anodic leakage current compared to CPE20 in chronoamperometry tests shown in **Figure 2-7** and **Figure 2-10**.

2.4 Summary

In conclusion, critical design principles were applied to modify conventional lithium metal polymer batteries (LMPs). First, to increase the ionic conductivity, liquid (DME) was added to polymer components to form a gel-polymer electrolyte. Additionally, to enhance anodic stability of this PEO-based gel-polymer electrolyte, salt concentration was increased to moderate degree (~3M). Lastly, PEO-based polymer matrix was modified into cross-linked structure by using in-situ polymerization of divinyl monomer, triethylene glycol divinyl ether (TEGDVE) to reduce diffusive flux of organic solvents into reactive cathode surface.

Regardless of polymer contents or polymer structure, solvation structures of liquid and gel electrolytes were all similar as confirmed by Raman

spectroscopic analysis. However, from chronoamperometry tests, it was revealed that anodic stability against NCM cathodes was highest in the electrolyte with cross-linked polymer matrix (CPE20). The origin of enhanced stability of CPE20 electrolyte was revealed by PFG-NMR confirming suppressed diffusion of DME molecules in polymer matrices. The suppression of solvent diffusion was found regardless of salt concentration. Although diffusion coefficients of DME molecules in electrolytes with linear chain polymer and cross-linked polymer matrix were similar, anodic stability was higher in cross-linked matrix due to diffusion of linear chain polymers increasing flux of organic components to oxidizing cathode surface.

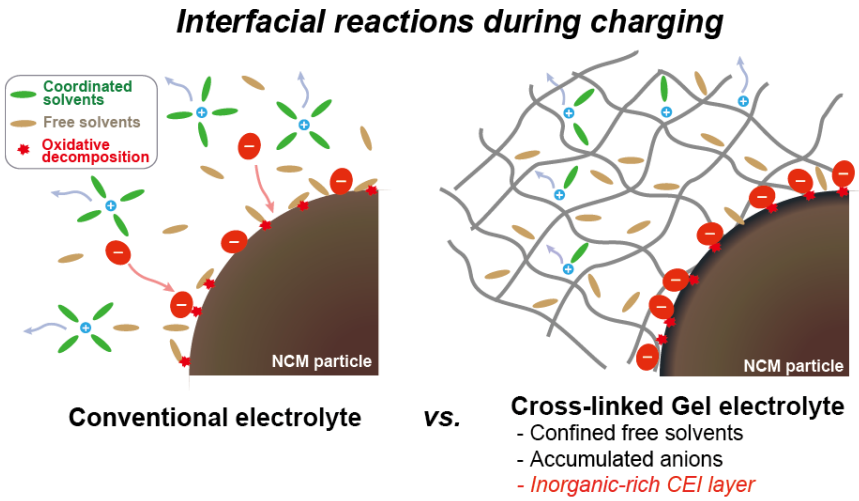

Figure 2-1. Comparison of interfacial reaction at cathodes in conventional liquid electrolyte and crosslinked gel electrolyte.

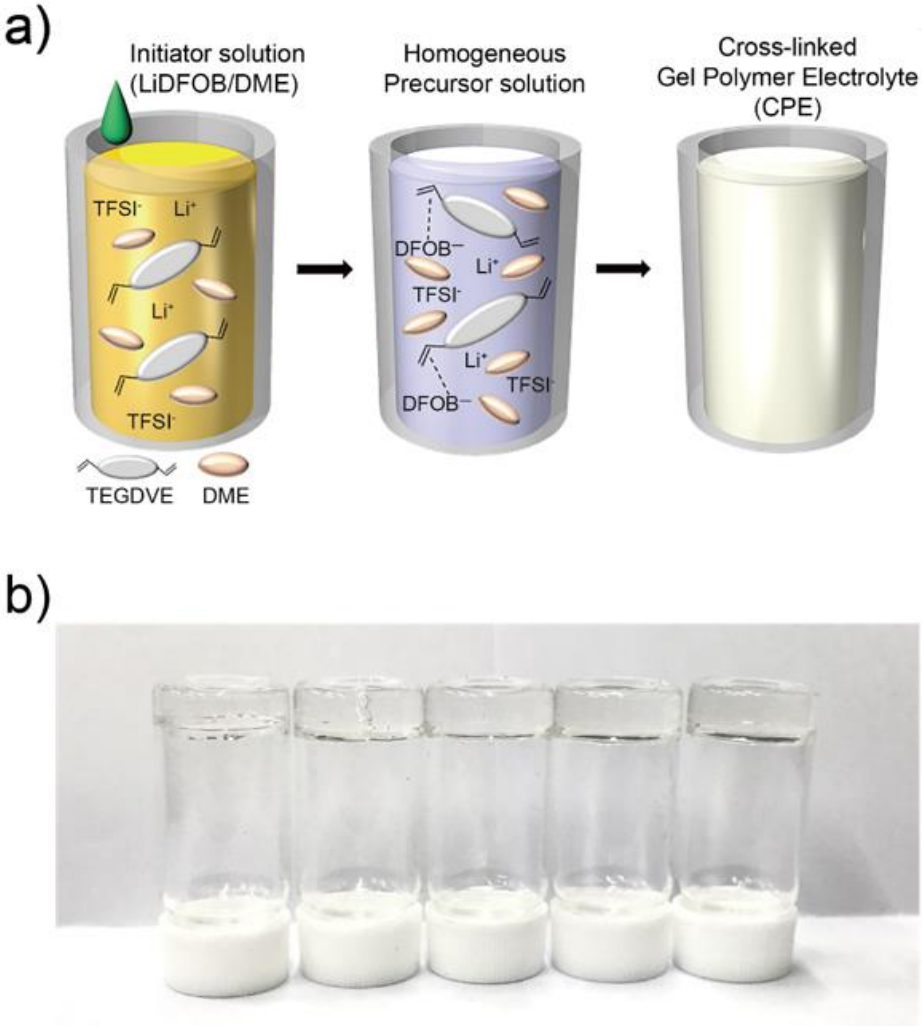

Figure 2-2. a) Schematic illustration for in-situ preparation of gel polymer electrolyte with cross-linkable monomer (TEGDVE). b) Optical images of polymerized CPEs with respective Li^+ concentrations (1.1, 1.8, 2.0, 2.7, 3.1M left to right).

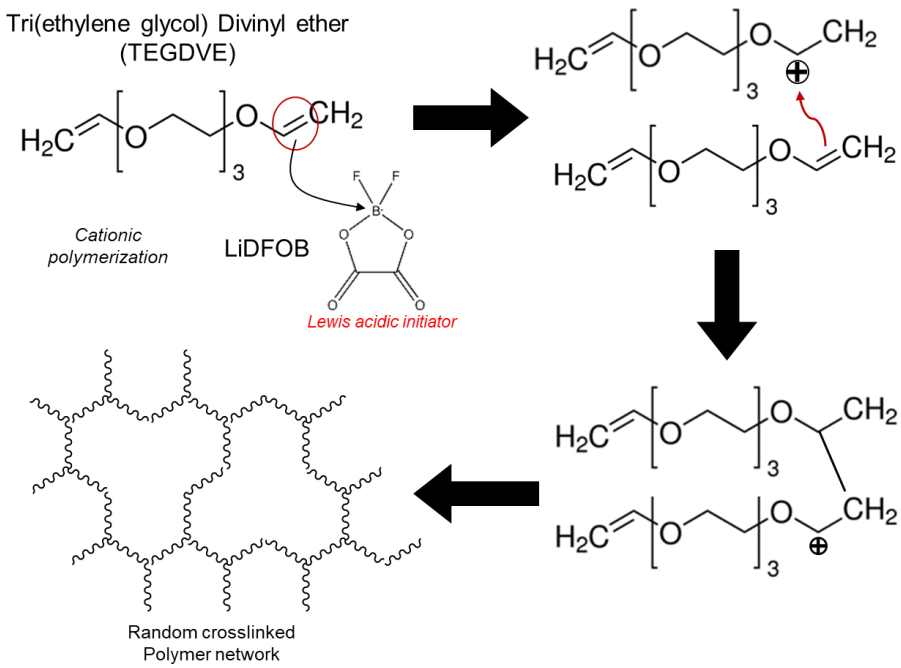

Figure 2-3. Reaction mechanism for cationic polymerization of cross-linkable TEGDVE monomer by lithium difluoro-oxalatoborate (LiDFOB) initiator.

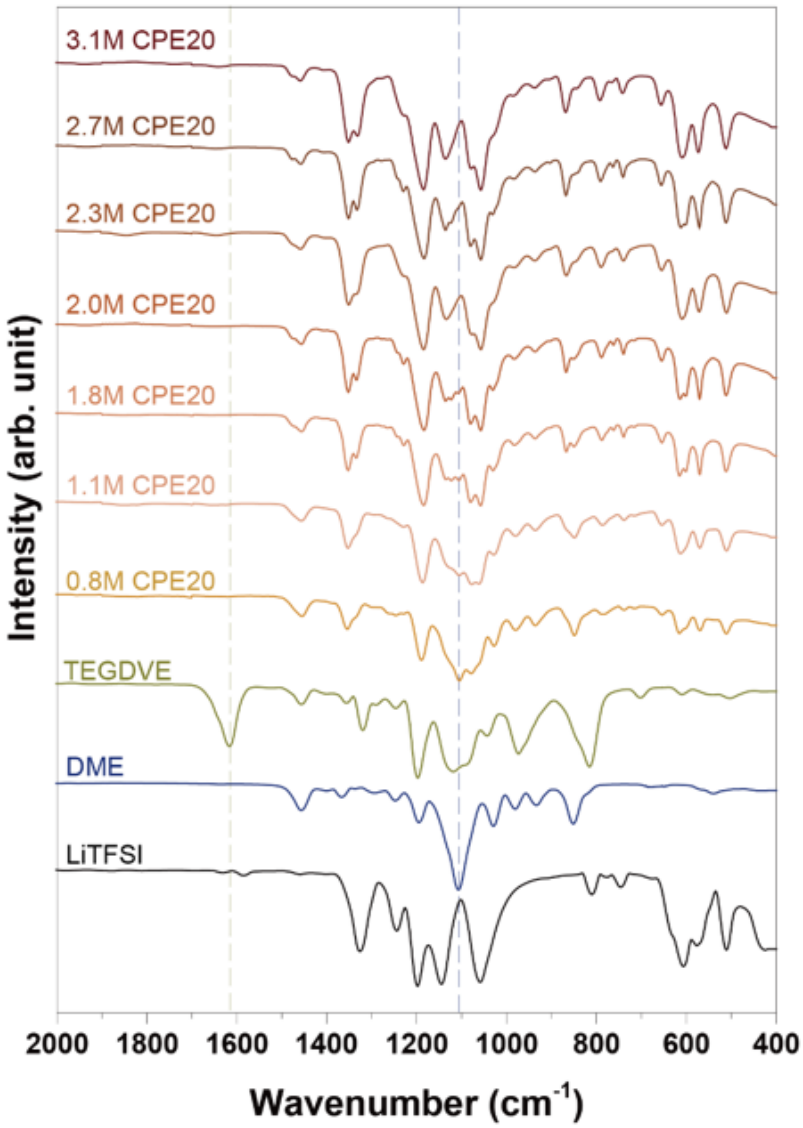

Figure 2-4. FT-IR spectra of cross-linked gel polymer electrolytes (CPEs) with respective concentrations.

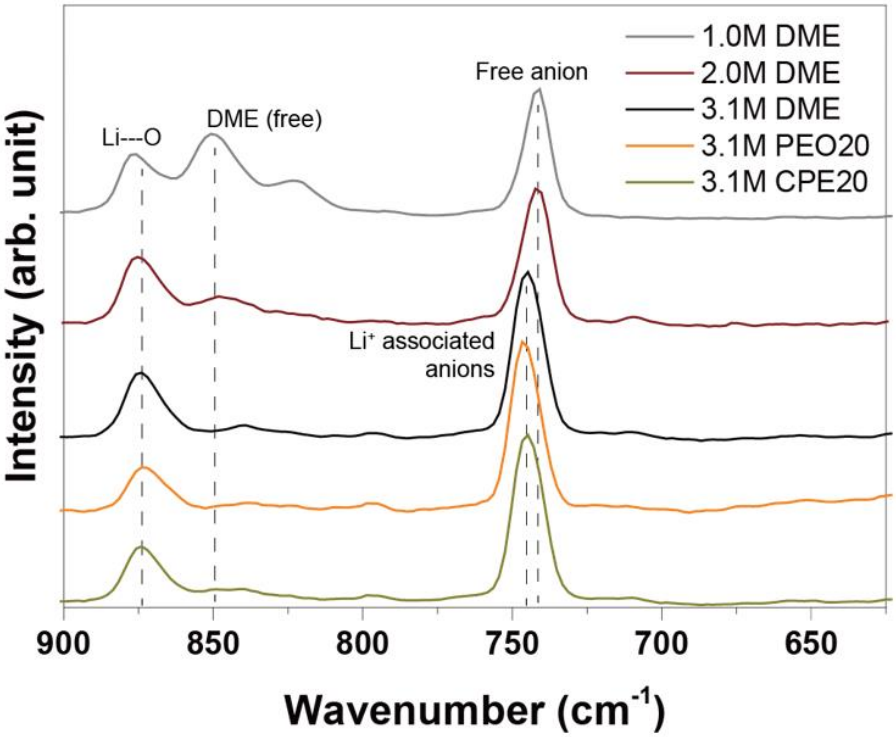

Figure 2-5. Raman spectra for each liquid and gel polymer electrolytes used in this study

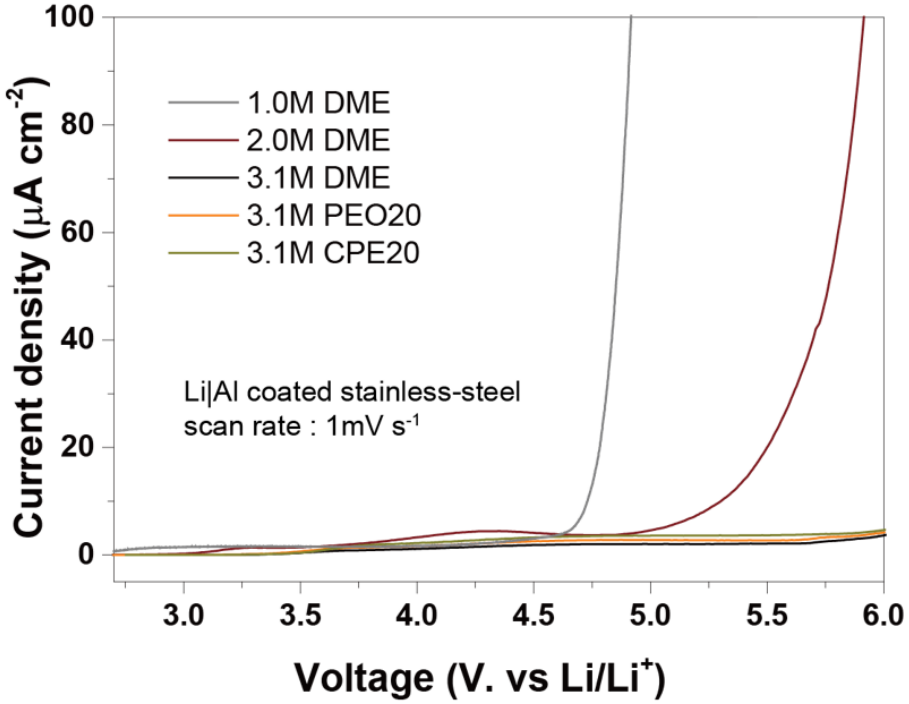

Figure 2-6. Linear sweep voltammograms for each liquid and gel polymer electrolytes to evaluate anodic stability

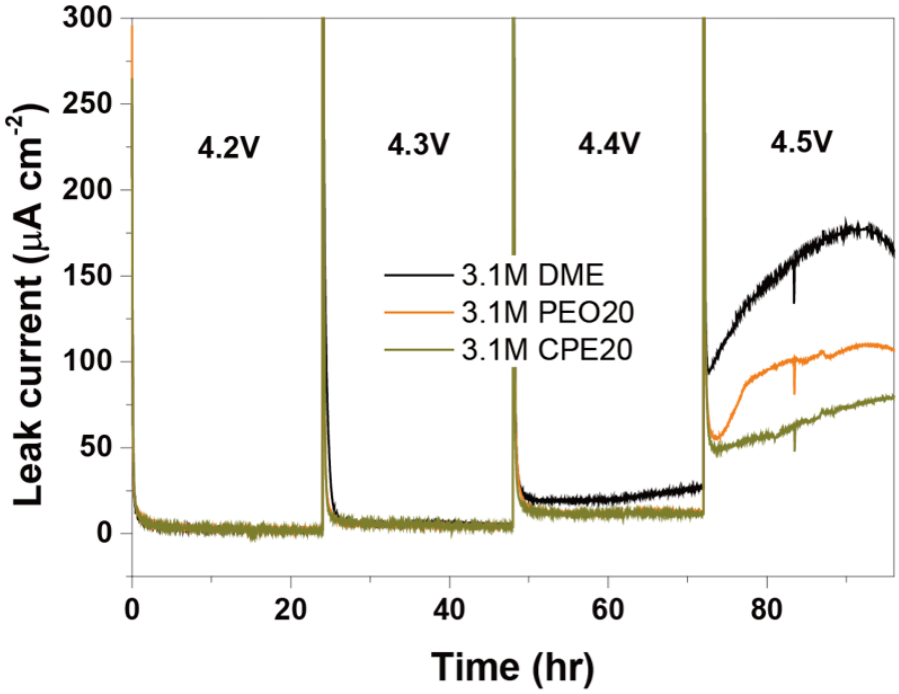

Figure 2-7. Chronoamperometry analysis for liquid and gel polymer electrolytes in high concentration (3.1 M).

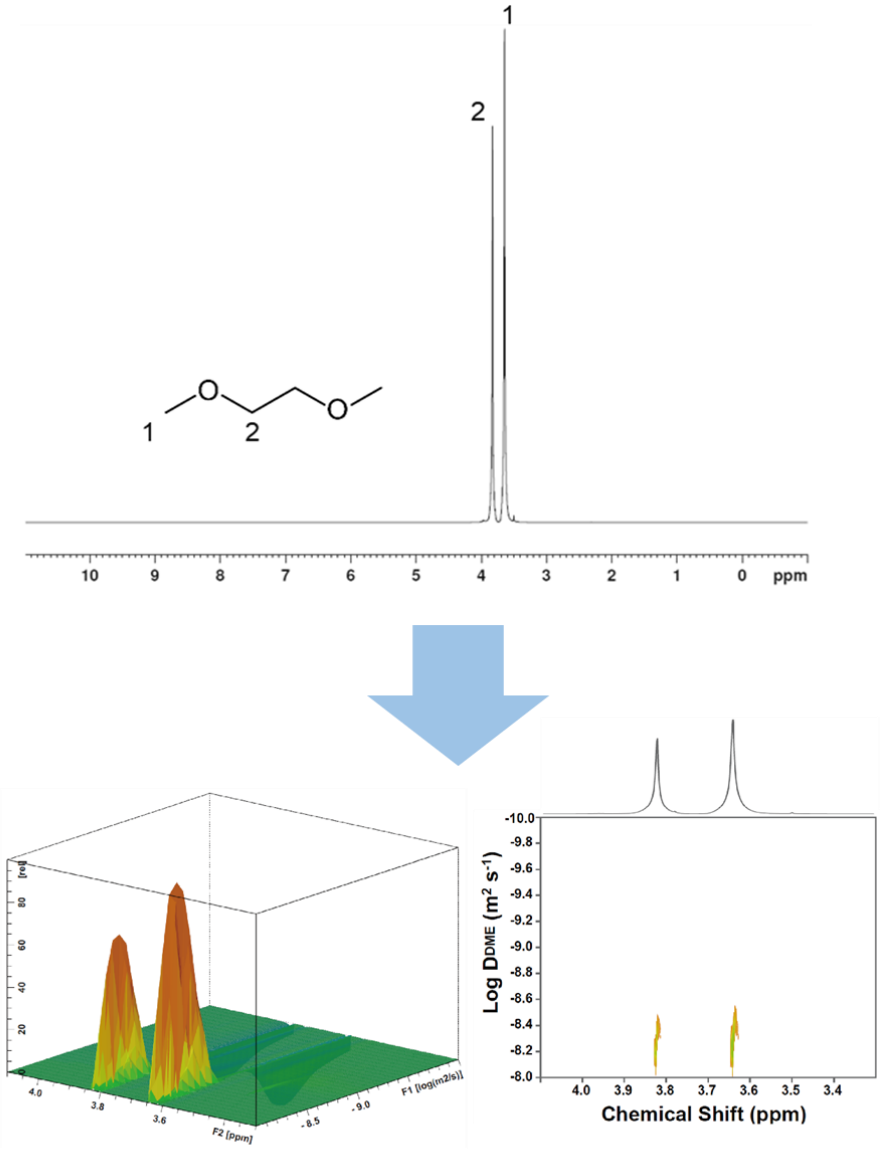

Figure 2-8. Schematic introduction for pulsed-field-gradient (PFG)-NMR analysis to measure diffusion coefficients of solvent molecules

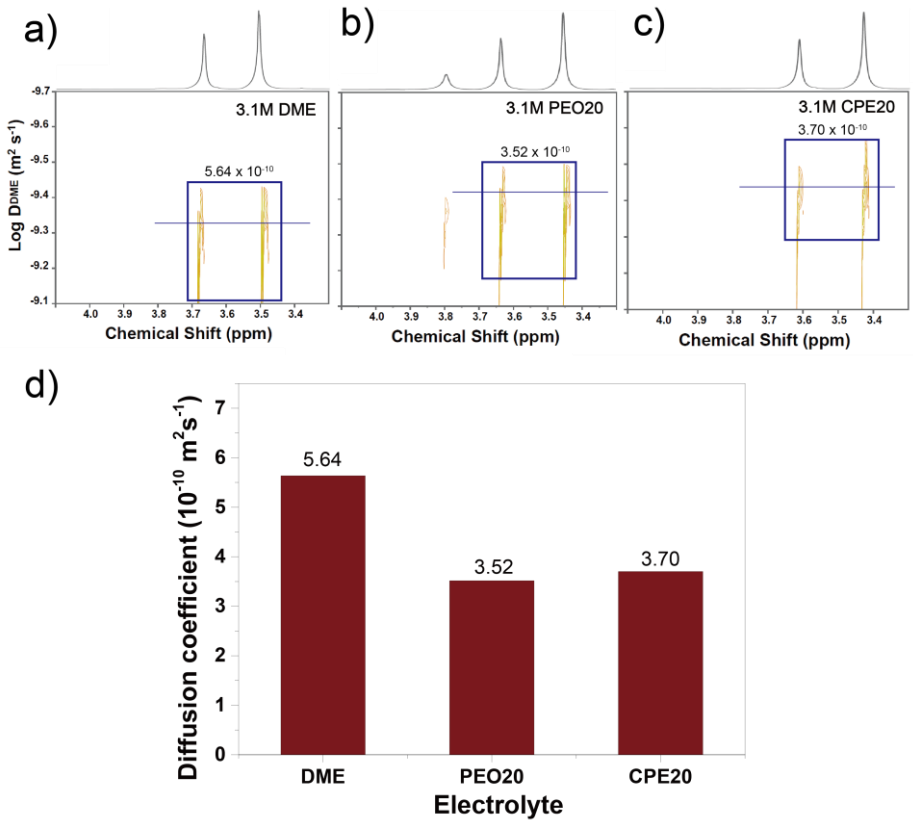

Figure 2-9. Diffusion coefficients of DME molecules in highly concentrated (3.1 M) liquid and gel polymer electrolytes measured by 1H PFG-NMR

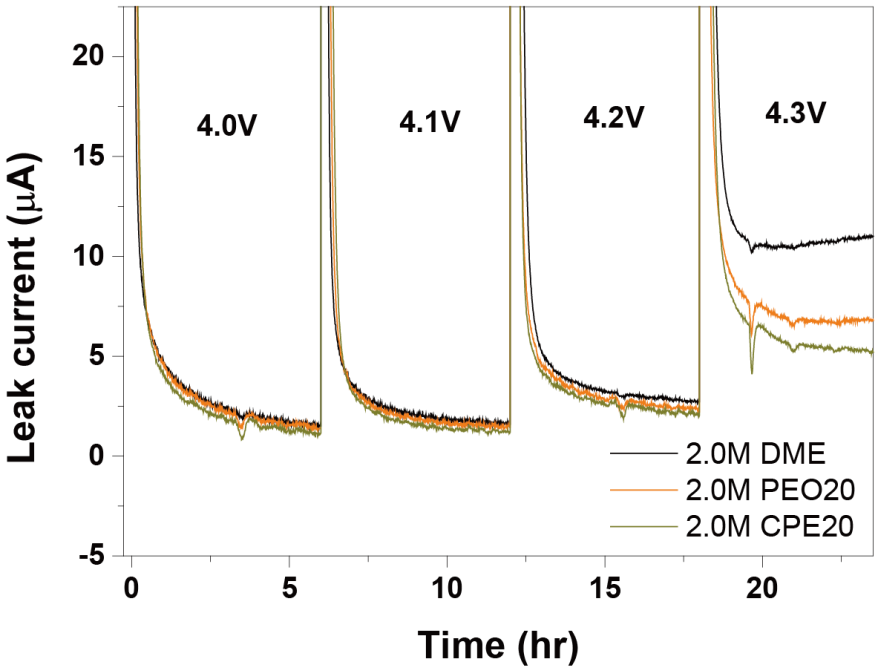

Figure 2-10. Chronoamperometry analysis for liquid and gel polymer electrolytes in lower concentration (2.0 M).

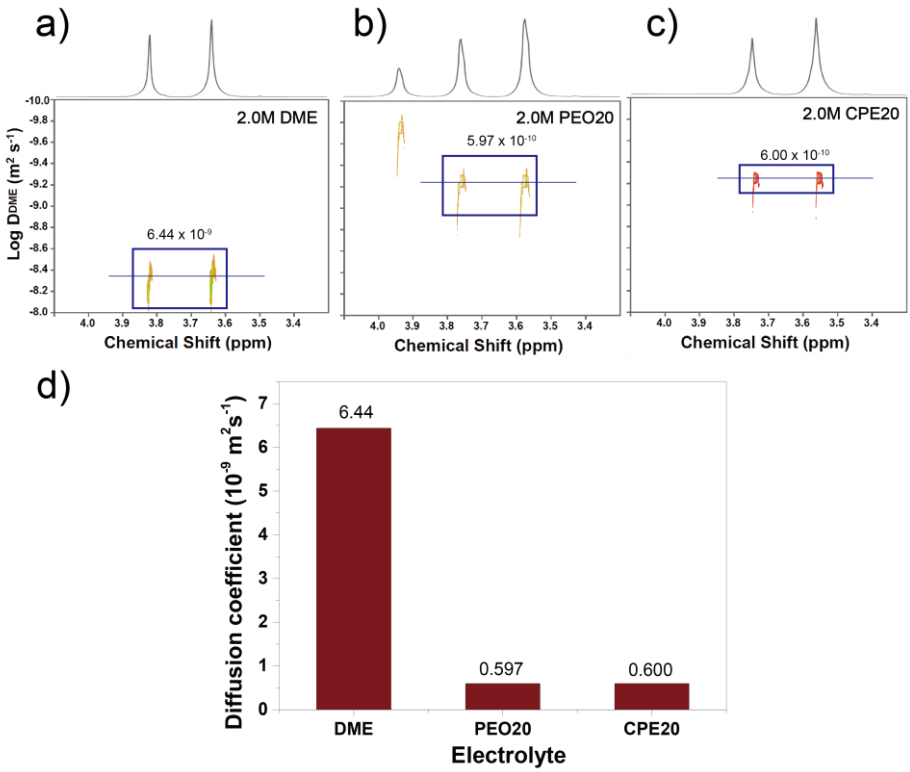

Figure 2-11. Diffusion coefficients of DME molecules in dilute (2.0 M) liquid and gel polymer electrolytes measured by 1H PFG-NMR

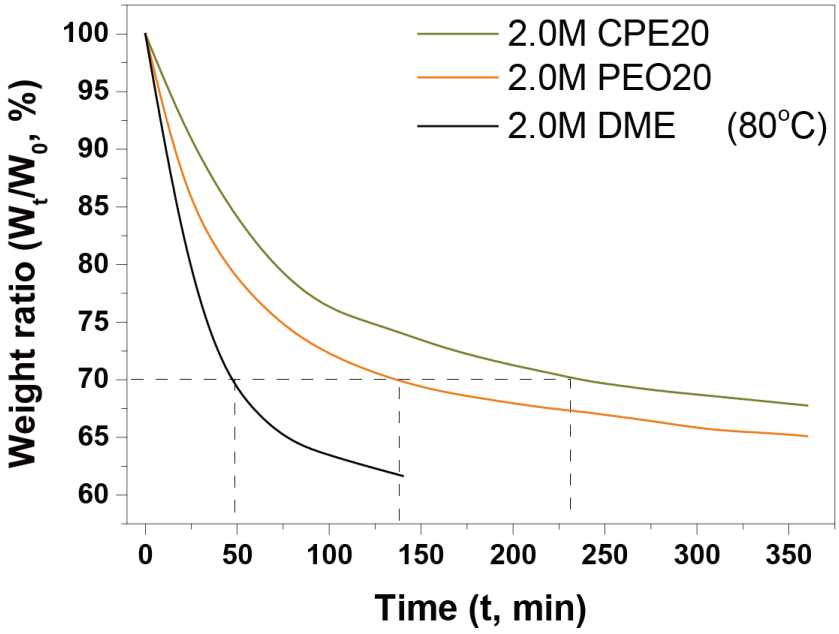

Figure 2-12. Isothermal thermogravimetric analysis (TGA) to compare the rate of DME evaporation in liquid and gel polymer electrolytes (2.0 M).

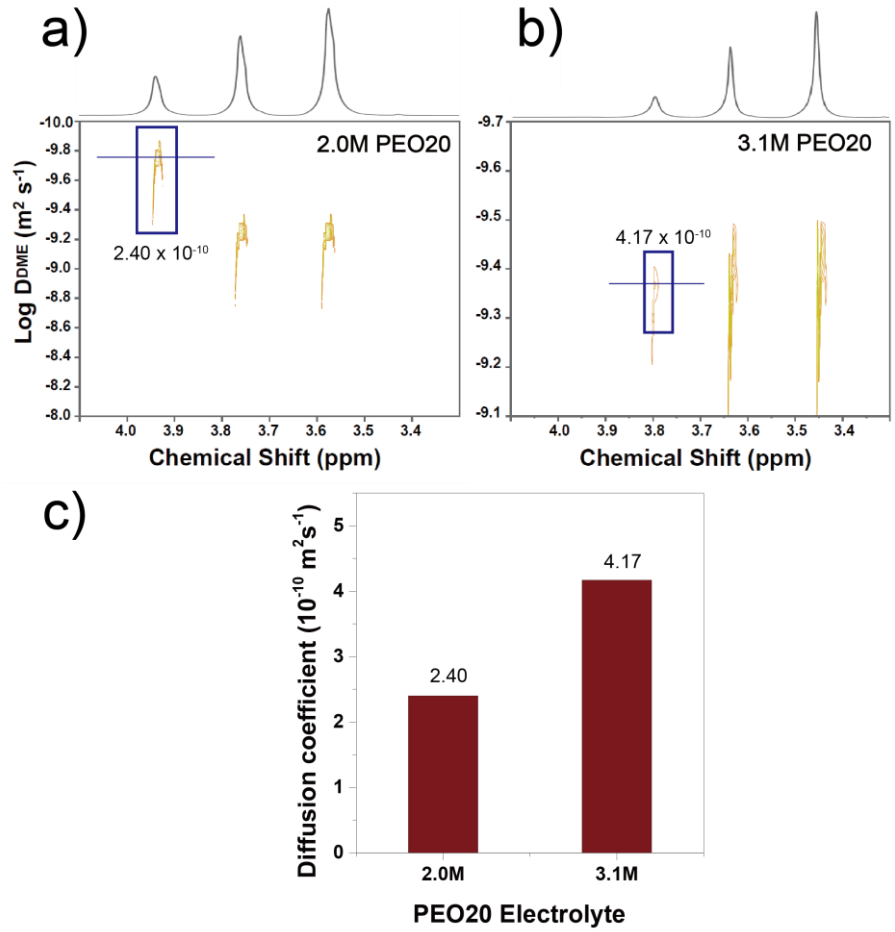

Figure 2-13. Diffusion coefficients of PEO polymer chains in 2.0M and 3.1M PEO20 electrolyte, respectively, measured by 1H PFG-NMR.

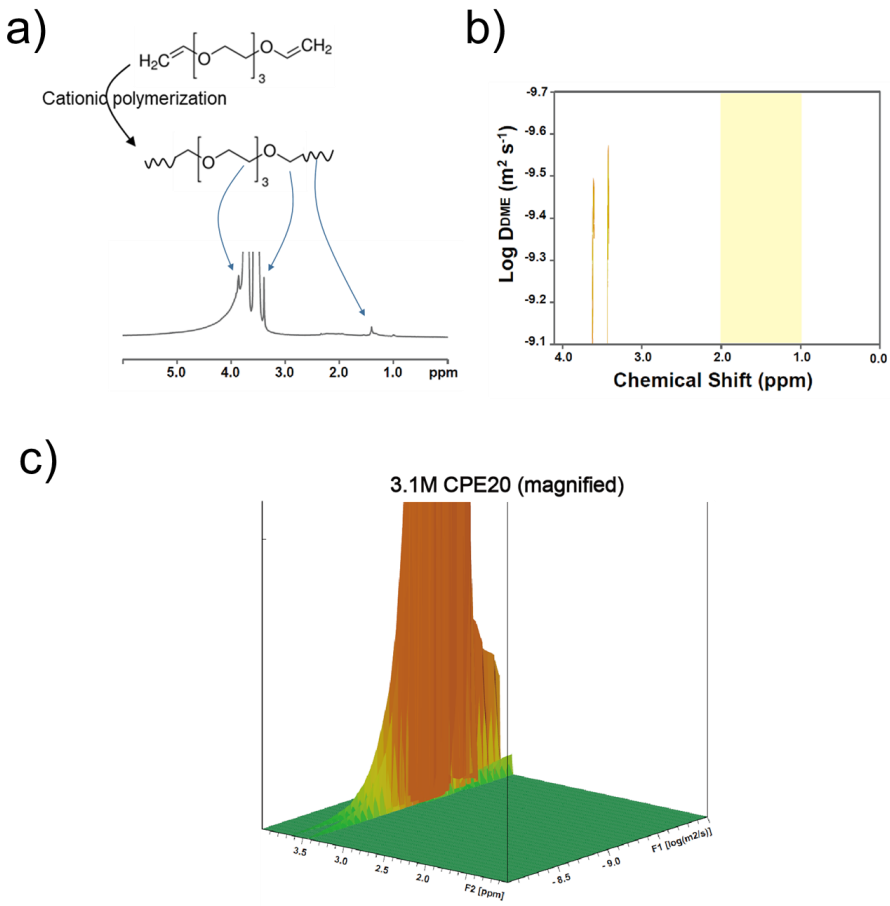

Figure 2-14. Diffusion coefficient of cross-linked polymer matrix in 3.1M CPE20 electrolyte indicating the absence of polymer diffusion in corresponding electrolyte.

3. Interfacial phenomena resulted from suppressed diffusion of solvents in Li metal batteries

3.1 Electrochemical performances of each electrolytes

In the previous chapter, it was confirmed that suppressing diffusive motion of solvent molecules by cross-linked polymer matrix can enhance anodic stability of gel electrolyte. The lower the amount of diffusing components in electrolyte, the higher the anodic stability of electrolyte is. This difference in anodic stability among liquid and gel electrolytes should be reflected in the electrochemical performances from various cell configurations.

Galvanostatic charge/discharge profiles of Li|NCM622 full cells with various electrolytes are shown in **Figure 3-1** and **Figure 3-2**. In **Figure 3-1-d)**, the rate of capacity decay is the slowest with CPE20 electrolyte. This result is originated from the correlation between decaying rate and the interfacial stability of cathode active materials with corresponding electrolyte. Slower capacity decay of Li|NCM622 cell indicates more stable interface between electrolyte and cathode materials has been formed.

Likewise, cross-linked gel electrolyte has shown the highest cyclic stability in Li|NCM622 cell among 2.0M DME, PEO20 and CPE20. However, a significant difference can be found compared to the results of 3.1M electrolytes. All the Li|NCM622 cells with 2.0M electrolytes are terminated by sudden death while the rate of gradual capacity decay was reflected by anodic

stability of each 3.1M electrolyte. This indicates interfacial stability of 2.0M electrolytes with Li metal has dominated the cyclic stability. Although significant difference has been found in anodic stabilities of 2.0M electrolytes, as shown in **Figure 2-10**, it acts as a minor factor in this case.

The superior full cell performances of CPE20 electrolytes are expected to be originated from interfacial phenomena. Consequently, it is highly required to thoroughly analyze and suggest interfacial phenomena causing significant differences in electrochemical performance of each electrolyte.

3.2 Interfacial analyses: cathodes

The electrochemical performances of cells in various conditions are determined by integrated effects from interfacial behaviors in both cathode and anode. Thus, it is highly required to conduct separate and thorough analysis for individual interfaces (electrolyte/cathode and electrolyte/anode). In previous chapters, three electrolytes were comparatively analyzed to study diffusional behavior of liquid solvent molecules in various polymeric matrices its correlation to anodic stability and, consequently, full cell performances. In **chapter 3.2** and **3.3**, interfacial behaviors of liquid and gel polymer electrolytes during full cell electrochemical cycling would be sequentially elucidated through post-mortem characterizations for cathode and anode.

NCM622 cathodes after galvanostatic charge/discharge tests with 3.1M liquid and gel polymer electrolytes were analyzed by XPS analysis, especially for fluorine element (**Figure 3-3**). Through XPS analysis, chemical compositions of surface (cathode electrolyte interphase, CEI layer) after interfacial reaction between cathode and electrolyte can be elucidated. In F1s spectra, chemical compositions vary significantly among 3.1M liquid and gel polymer electrolytes. On the surface of NCM cathodes cycled with 3.1M DME electrolyte, relative amount of Li-F (~685 eV) compared to C-F (~687 eV, originated from PVDF binder) is the weakest among cathodes cycled with various electrolytes. The relative intensity of Li-F is the strongest on cathodes cycles with 3.1M CPE20 electrolyte. The higher composition of Li-F in CEI layer indicates its inorganic-rich and robust nature since formation of Li-F on interfacial layer is enriched as anions participate more in the interfacial reaction. The highest relative amount of Li-F in CEI formed by 3.1M CPE20 proves the design principle introduced in **figure 2-1** worked as expected, suppressing diffusive flux of liquid molecules in cross-linked matrix to promote participation of anions in CEI formation. This inorganic-rich and robust CEI layer improves anodic stability of electrolyte by alleviating oxidative degradation and subsequently enhances overall cyclic stability as shown in **figure 3-1**.

Confined diffusion of liquid molecules in cross-linked polymer matrix was also confirmed in electrolytes with lower concentration (**Figure 2-11**). In

accordance with previous results from XPS analyses, Li-F was the most enriched in CEI layer on cathodes cycles with cross-linked gel polymer electrolyte among various 2.0M liquid and gel electrolytes (**Figure 3-4**). As for 3.1M electrolytes, cross-linked polymeric matrix in 2.0M CPE20 also suppresses diffusive flux of solvent molecules to reactive cathode interface and allow anions contribute more to the formation of CEI layer.

It can be concluded that, regardless of salt concentration, polymeric matrix, especially cross-linked one, can induce robust and inorganic-rich CEI layer by reducing diffusive flux of liquid molecules during the interfacial reaction. This proves the design principle of this study effective for enhancing anodic stability of electrolytes against high voltage cathodes.

3.3 Interfacial analyses: anodes

Cyclic stability of electrolytes in full cell configurations are determined by integrated effects from interfacial phenomena both at cathode and anode. In addition to anodic stability, cathodic stability against lithium metal has a significant influence on cyclic stability of electrolytes.

To evaluate cathodic stability of various liquid and gel electrolytes without any influence of anodic stability against NCM electrodes, galvanostatic charge/discharge of Li|Li symmetric cells were conducted with 3.1M liquid and gel electrolytes at current densities of 0.5, 1.0mA cm^{-2} and areal capacity of 1.0

mAh cm^{-2} (**Figure 3-5**). Cyclic stabilities of Li|Li charge/discharge were similar with 3.1M DME and CPE20 although overpotential was lower with 3.1M DME due to higher ionic conductivity. With 3.1M PEO20 electrolyte, Li|Li symmetric cell was the most unstable and failed most rapidly.

Since the determining factors for cathodic stability against Li metal differ from anodic stability against NCM cathodes, a varied approach is required to elucidate the origin of cathodic stability gap between liquid and gel electrolytes. First, similarly in the evaluation of oxidative stability, chemical composition of SEI layer also acts as a major determining factor for stable electrochemical cycling of Li metal. In addition, mechanical strength applied to Li metal also significantly influence on the same phenomenon.

Correspondingly, chemical composition of SEI layers on Li metals cycled with 3.1M liquid and gel electrolytes were analyzed by X-ray photoelectron spectroscopy (**Figure 3-6**). In order to stabilize SEI layer, it is also advantageous to induce inorganic-rich components, especially Li-F components. It can be determined from XPS, especially F1s spectra which anions participate in the interfacial reaction with Li metal. Each peak at ~688eV and ~685eV indicates C-F bond and Li-F bond, respectively resulted from decomposition of anions in LiTFSI and LiDFOB. As shown in **figure 3-6**, the amount of Li-F is the lowest in the SEI formed by 3.1M CPE20 electrolyte compared to those formed by 3.1M DME and PEO20 electrolytes. This difference indicates dominant participation of LiDFOB in the formation of

anode SEI layer in 3.1M DME and PEO20 while LiTFSI dominates in 3.1M CPE20. Since most of added DFOB anions are consumed during in-situ polymerization in CPE20, relatively lower amounts of DFOB anions are available during electrochemical charge/discharge. In contrast, since all of initially added DFOB anions are intact in DME and PEO20 electrolytes which do not go through any polymerization reaction that consumes DFOB anions, those are completely available for interfacial reaction during electrochemical charge/discharge. In spite of lower amount of advantageous Li-F in anode SEI formed by 3.1M CPE20, cyclic stability of Li|Li symmetric cell with 3.1M CPE20 is much higher than that with 3.1M PEO20, and similar to that with 3.1M DME electrolyte. This result indicates a critical factor other than chemical composition of SEI mainly determined the cyclic stability of Li metal in each liquid and gel polymer electrolytes.

In order to discover the determining factor for anode stability, morphology analyses were conducted with scanning electron microscope. Surface morphology of Li metals after cycled in Li|NCM cells with 3.1M liquid and gel electrolytes were analyzed by SEM (**Figure 3-7**). The largest lateral growth of Li is induced with 3.1M CPE20 while whisker-like porous morphologies have been formed with 3.1M DME and PEO20. Additionally, it is confirmed that formation of compact-planar Li morphology is related to the type of polymeric matrix rather than salt concentration as shown in SEM analyses of deposited Li after 1st charge of Cu|NCM cells with 2.0M liquid and

gel polymer electrolytes (**Figure 3-8**). Among 2.0M DME, PEO20 and CPE20 electrolytes, only CPE20 electrolytes induced compact-planar Li morphology after deposition of Li on Cu current collector.

According to Itkis et al., Li can be deposited into planar morphology by atomic diffusion of Li through grain boundaries into metal bulk.[31] Since this planar growth by extension of grain base accumulates stress on the surface, additional nucleates become newly formed and whisker-like morphologies grow further. To further extend the planar growth of Li, higher mechanical strength should be applied on Li surface. It can be inferred that the highest mechanical strength applied to Li metal by CPE20 due to cross-linked polymeric matrix enabled the largest lateral growth of Li with CPE20 compared to DME or PEO20 electrolytes. Therefore, it can be concluded that high cyclic stability of CPE20 electrolytes is originated from the highest mechanical strength in spite of lowest amounts of advantageous SEI components among liquid and gel polymer electrolytes.

3.4 Summary

Followed by previous chapter, electrochemical performances and interfacial phenomena were thoroughly analyzed by XPS and SEM. Cyclic stability of Li|NCM622 cell was the highest with CPE20 electrolyte regardless of salt concentration (2.0 and 3.1M). To discover the origin of electrochemical

performances, interface analyses were conducted respectively for cathodes and anodes after cycled with DME, PEO20 and CPE20 electrolytes. Since diffusion of solvent molecules to cathode was highly suppressed during charging with CPE20 electrolytes, anions predominantly participated in the formation of CEI layer and formed robust inorganic-rich CEI layer compared to those by DME or PEO20 electrolytes. Anode SEI stability could also be acquired with CPE20 electrolytes by different origin from CEI layer. Although cyclic stability of Li|Li cell was the lowest with PEO20 electrolyte, advantageous Li-F content was rather higher in SEI than that of CPE20 electrolyte. Through morphology analyses by SEM, it was discovered that planar growth and consequent anode stability by CPE20 was resulted by high mechanical strength of cross-linked polymeric matrix in CPE20. The respective interfacial phenomena (advantageous components in CEI and mechanical strength applied to Li metal) resulted in the highest electrochemical performance of Li|NCM622 cell with CPE20 electrolytes.

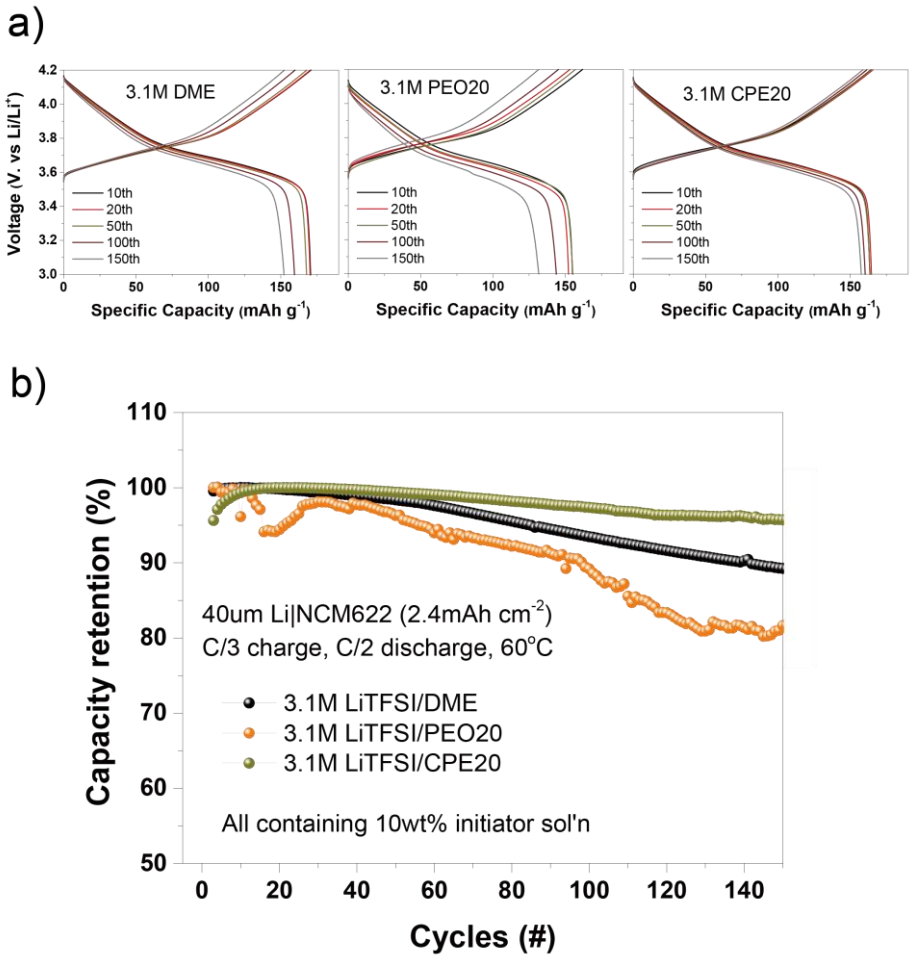

Figure 3-1. Full cell (Li|NCM) cycling with 3.1 M liquid and gel polymer electrolytes at 60°C.

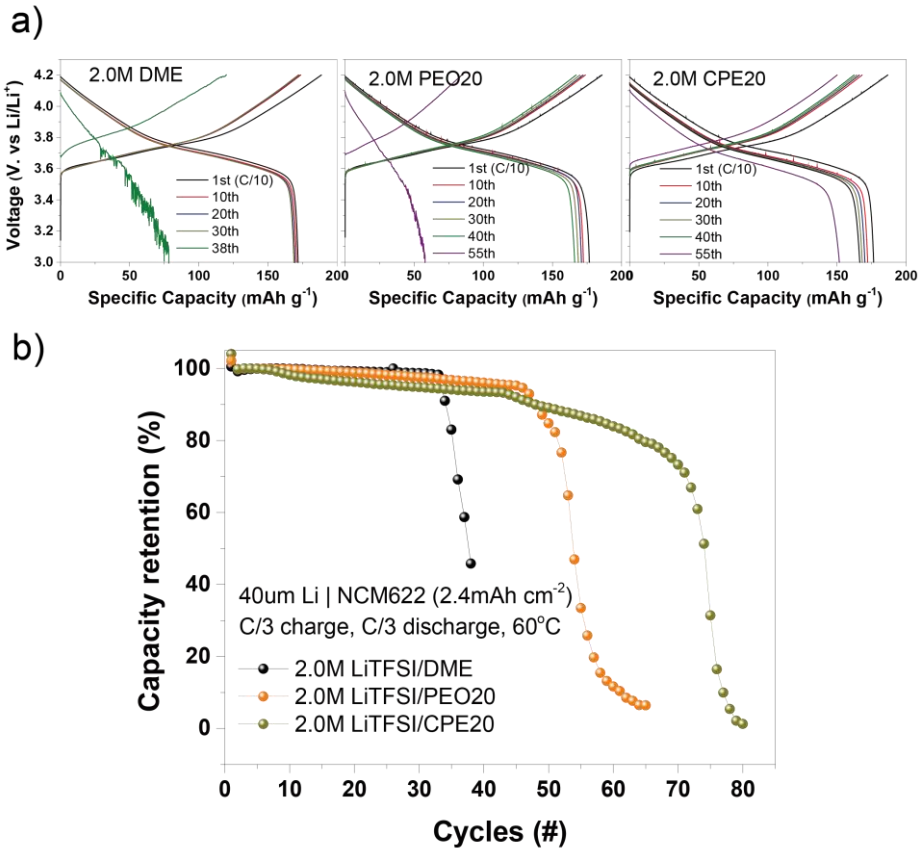

Figure 3-2. Full cell (Li|NCM) cycling with 2.0 M liquid and gel polymer electrolytes at 60°C.

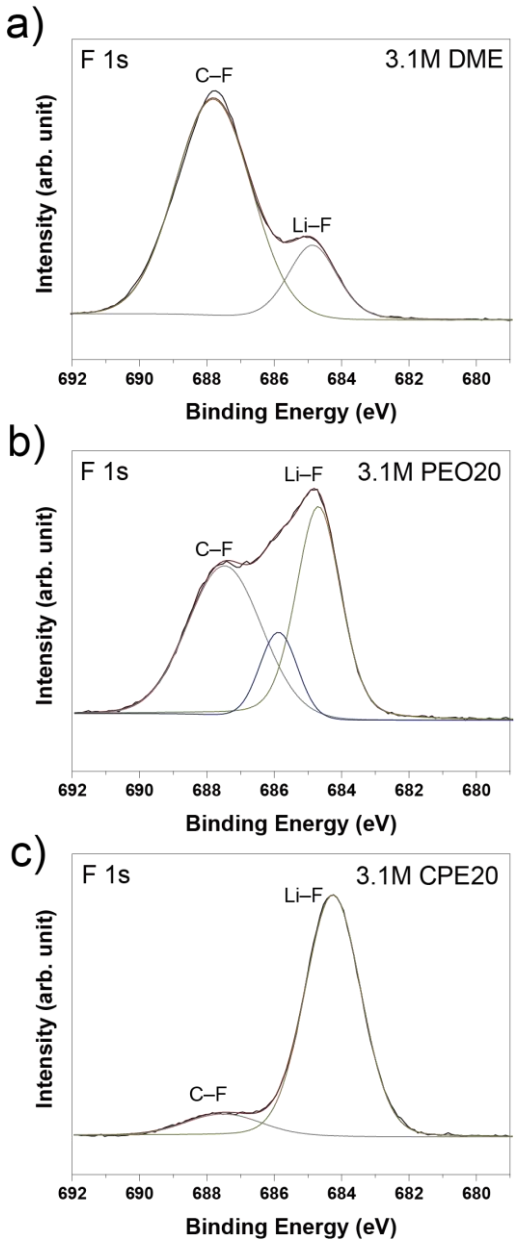

Figure 3-3. F 1s XPS spectra of NCM622 electrodes after 20 cycles with 3.1 M liquid and gel polymer electrolytes.

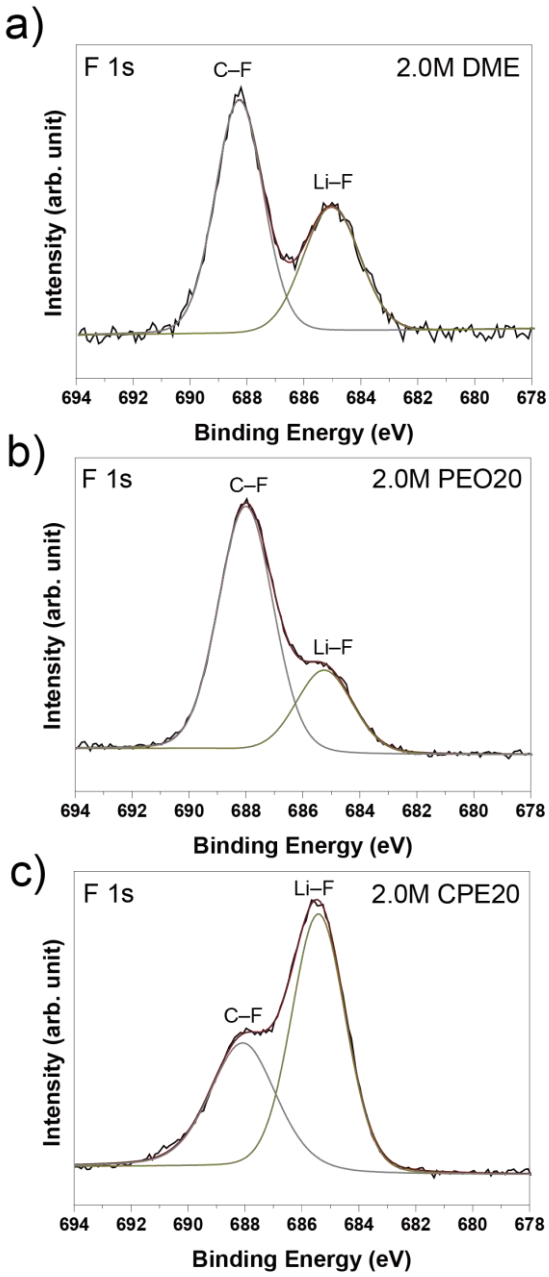

Figure 3-4. F 1s XPS spectra of NCM622 electrodes after 20 cycles with 2.0 M liquid and gel polymer electrolytes.

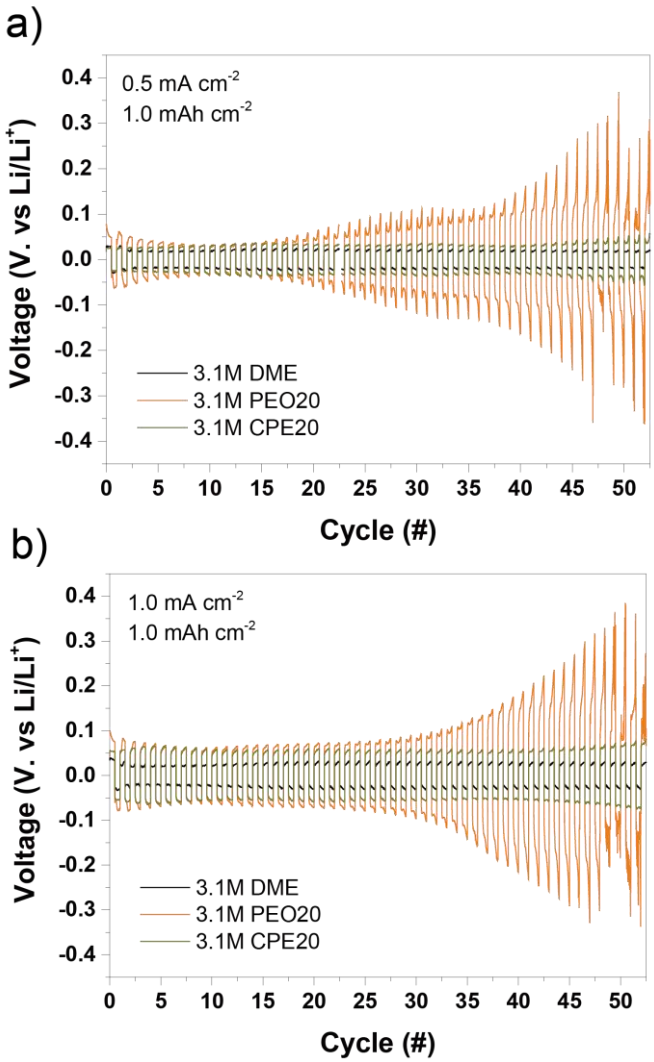

Figure 3-5. Li|Li symmetric cell cycling tests with 3.1 M liquid and gel polymer electrolytes under various current and areal specific capacity.

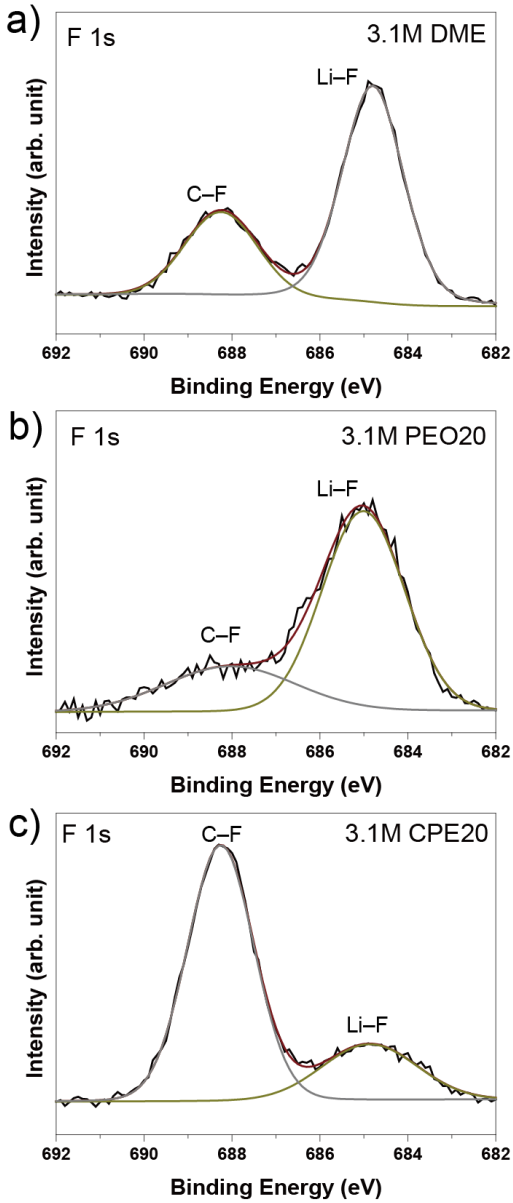

Figure 3-6. F1s XPS spectra of Li metal surfaces after cycled with 3.1M liquid and gel polymer electrolytes.

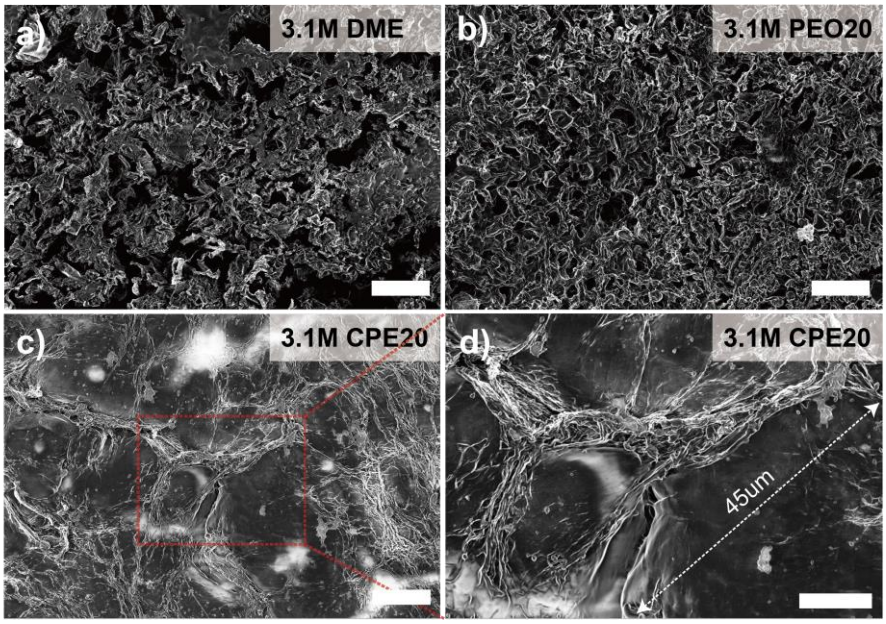

Figure 3-7. SEM images of Li surface morphology after 20 cycles in Li|NCM full cells with respective electrolytes, a)-c), magnified SEM image of Li surface after 20 cycles in Li|NCM with 3.1 M CPE20 electrolyte, d). Scale bars are 20μm for a)-c), and 10μm for d).

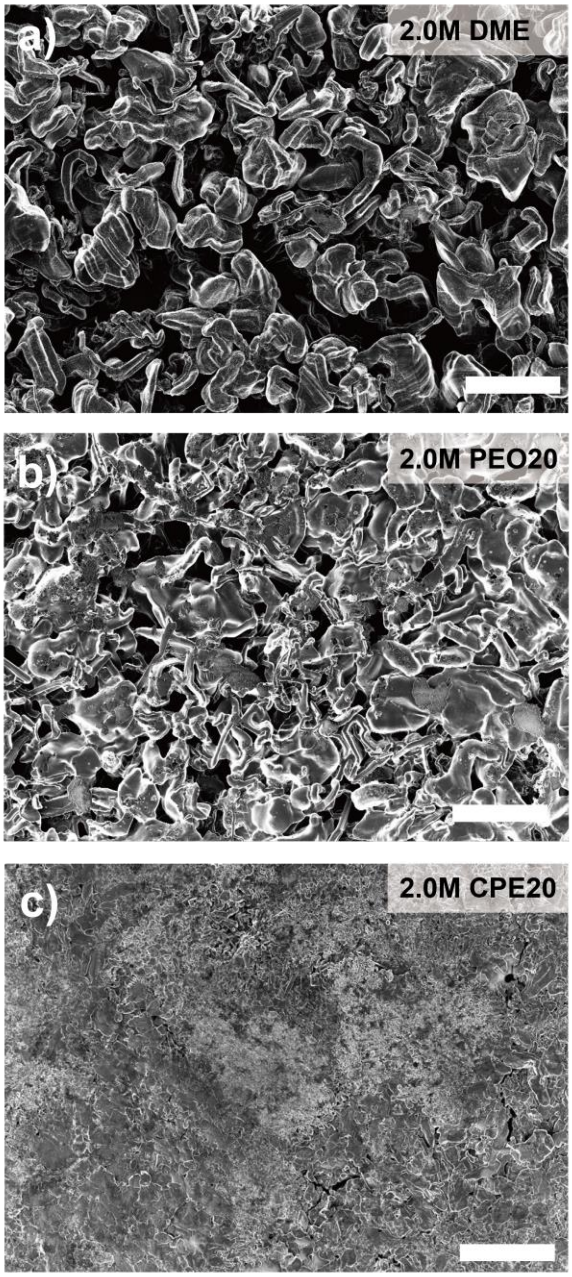

Figure 3-8. Li plated on Cu in Cu|NCM coin cells after 1st charge with 2.0 M liquid and gel polymer electrolytes. Scale bars are 50μm.

4. Summary and Conclusions

Li metal batteries have drawn a sharp interest since the Li metal anode provides a lot higher specific capacity (3860 mAh g^{-1}) compared to commercial graphite anode (370 mAh g^{-1}). Due to its high theoretical specific capacity, lithium metal is highly expected to achieve the minimum target energy density of post Li-ion batteries (500 Wh/kg). However, due to high reactivity of Li metal, uncontrolled interfacial reaction results in dendritic growth of Li metal, and subsequently, various problems such as safety hazard by short-circuiting, degraded energy density, and increased cell impedances. Consequently, various strategic approaches have been developed and Li metal batteries have been improved to some extent. By virtue of these enthusiastic challenges, Li metal polymer batteries have been even commercialized for electric vehicle applications by French Motor company, Bolloré. However, its features were far less than target energy density to become the real 'post Li-ion' and still it left challenging limitations to overcome.

Based on the serious limitations of previously commercialized Li metal polymer batteries, in this study, systematic design principles were constructed and employed comprehensively to develop high voltage lithium metal polymer batteries. 1) To resolve high cell impedance from low ionic conductivity of solid polymer electrolytes, liquid solvents (1,2-dimethoxyethane) was incorporated into the electrolyte. To retain the

electrolyte to be compatible with Li metal, ether-based polymer and liquid solvents were utilized as in the Bolloré battery. 2) To compensate for the low anodic stability of ether based components, lithium salts were concentrated (~3.1M) and cross-linked polymeric matrix were employed to suppress diffusive flux of solvent molecules to reactive cathode surface, and consequently form robust inorganic-rich CEI layer for sustainable interfacial stability at cathode.

Three electrolytes were prepared and comparatively studied: Li salts in DME, DME with polyethylene oxide, and DME with cross-linked polyethylene oxide in same salt concentrations. Each electrolyte represents for liquid electrolyte, gel polymer electrolyte with linear polymer chains, and cross-linked gel polymer electrolyte. To prepare cross-linked gel electrolyte, ether-based triethylene glycol divinyl ether was employed as monomer to be in-situ polymerized by cationic initiator lithium difluoro-oxalatoborate (LiDFOB) salt. To prove initial hypothesis that diffusion of solvent molecules would be suppressed in cross-linked polymeric matrix, pulsed-field gradient NMR (PFG-NMR) spectroscopic analysis was conducted for liquid and gel polymer electrolytes to evaluate diffusive motion of solvents in each electrolyte. As expected, diffusion of solvent molecules was highly suppressed in cross-linked polymeric matrix compared to that in liquid and linear chain gel polymer electrolyte. Additionally, not only solvent molecules, but also linear polymer chains were found to diffuse in corresponding gel electrolyte while the absence

of polymer diffusion in cross-linked gel electrolyte was revealed by PFG-NMR analysis.

To confirm the correlation between diffusion of solvent molecules and electrochemical performances, Li|NCM cells with liquid and gel electrolytes were tested under constant current charge/discharge. Regardless of salt concentration, cyclic stability of Li|NCM cell was the highest with cross-linked gel electrolytes. Through the respective analyses of cathode and anode after Li|NCM charge/discharge cycling tests, different interfacial phenomena were induced by each electrolyte. Due to suppressed diffusion of solvent molecules in cross-linked gel electrolyte, anions contribute dominantly to the formation of robust inorganic-rich CEI layer to enhance oxidative stability of electrolyte. In the Li metal anode side, mechanically suppressed dendrite growth by cross-linked gel electrolyte contributes to stable electrochemical performance rather than chemical advantages. Finally, it was confirmed that design principles constructed and utilized in this study, worked properly as evidenced by various spectroscopic and interface analyses.

5. Bibliography

[1] a) R. Eisenberg, H. B. Gray, G. W. Crabtree, *Proceedings of the National Academy of Sciences* **2020**, 117, 12543; b) B. K. Sovacool, P. Schmid, A. Stirling, G. Walter, G. MacKerron, *Nature Energy* **2020**, 5, 928.

[2] a) P. Albertus, S. Babinec, S. Litzelman, A. Newman, *Nature Energy* **2018**, 3, 16; b) European Council for Automotive R&D, 2019.

[3] a) M. He, R. Guo, G. M. Hobold, H. Gao, B. M. Gallant, *Proceedings of the National Academy of Sciences* **2020**, 117, 73; b) X.-B. Cheng, R. Zhang, C.-Z. Zhao, Q. Zhang, *Chemical Reviews* **2017**, 117, 10403.

[4] R. Pathak, K. Chen, A. Gurung, K. M. Reza, B. Bahrami, J. Pokharel, A. Baniya, W. He, F. Wu, Y. Zhou, K. Xu, Q. Qiao, *Nature Communications* **2020**, 11, 93.

[5] C. Fang, X. Wang, Y. S. Meng, *Trends in Chemistry* **2019**, 1, 152.

[6] D. Lin, Y. Liu, Z. Liang, H.-W. Lee, J. Sun, H. Wang, K. Yan, J. Xie, Y. Cui, *Nature nanotechnology* **2016**, 11, 626.

[7] a) D. J. Yoo, A. Elabd, S. Choi, Y. Cho, J. Kim, S. J. Lee, S. H. Choi, T. w. Kwon, K. Char, K. J. Kim, *Advanced Materials* **2019**, 31, 1901645; b) S. Choi, T.-w. Kwon, A. Coskun, J. W. Choi, *Science* **2017**, 357, 279.

[8] L.-L. Lu, J. Ge, J.-N. Yang, S.-M. Chen, H.-B. Yao, F. Zhou, S.-H. Yu,

Nano Letters **2016**, 16, 4431.

[9] a) C. Niu, H. Pan, W. Xu, J. Xiao, J.-G. Zhang, L. Luo, C. Wang, D. Mei, J. Meng, X. Wang, Z. Liu, L. Mai, J. Liu, *Nature Nanotechnology* **2019**, 14, 594; b) H. Wang, J. Wu, L. Yuan, Z. Li, Y. Huang, *ACS Applied Materials & Interfaces* **2020**, 12, 28337; c) J. Pu, J. Li, K. Zhang, T. Zhang, C. Li, H. Ma, J. Zhu, P. V. Braun, J. Lu, H. Zhang, *Nature Communications* **2019**, 10, 1896; d) P. Xue, S. Liu, X. Shi, C. Sun, C. Lai, Y. Zhou, D. Sui, Y. Chen, J. Liang, *Advanced Materials* **2018**, 30, 1804165; e) L. Luo, J. Li, H. Yaghoobnejad Asl, A. Manthiram, *Advanced Materials* **2019**, 31, 1904537; f) H. Wang, D. Lin, J. Xie, Y. Liu, H. Chen, Y. Li, J. Xu, G. Zhou, Z. Zhang, A. Pei, Y. Zhu, K. Liu, K. Wang, Y. Cui, *Advanced Energy Materials* **2019**, 9, 1802720; g) X. Qian, X. Fan, Y. Peng, P. Xue, C. Sun, X. Shi, C. Lai, J. Liang, *Advanced Functional Materials* **2021**, 31, 2008044.

[10] K. Liu, A. Pei, H. R. Lee, B. Kong, N. Liu, D. Lin, Y. Liu, C. Liu, P.-c. Hsu, Z. Bao, Y. Cui, *Journal of the American Chemical Society* **2017**, 139, 4815.

[11] Y. Gao, Z. Yan, J. L. Gray, X. He, D. Wang, T. Chen, Q. Huang, Y. C. Li, H. Wang, S. H. Kim, T. E. Mallouk, D. Wang, *Nature Materials* **2019**, 18, 384.

[12] C. Fu, V. Venturi, J. Kim, Z. Ahmad, A. W. Ells, V. Viswanathan, B. A. Helms, *Nature Materials* **2020**, 19, 758.

[13] a) J. Qian, W. A. Henderson, W. Xu, P. Bhattacharya, M. Engelhard, O. Borodin, J.-G. Zhang, *Nature Communications* **2015**, 6, 6362; b) V. Nilsson, A. Kotronia, M. Lacey, K. Edström, P. Johansson, *ACS Applied Energy Materials* **2020**, 3, 200; c) S. Jiao, X. Ren, R. Cao, M. H. Engelhard, Y. Liu, D. Hu, D. Mei, J. Zheng, W. Zhao, Q. Li, N. Liu, B. D. Adams, C. Ma, J. Liu, J.-G. Zhang, W. Xu, *Nature Energy* **2018**, 3, 739; d) L. Suo, W. Xue, M. Gobet, S. G. Greenbaum, C. Wang, Y. Chen, W. Yang, Y. Li, J. Li, *Proceedings of the National Academy of Sciences* **2018**, 115, 1156.

[14] X. Cao, H. Jia, W. Xu, J.-G. Zhang, *Journal of The Electrochemical Society* **2021**, 168, 010522.

[15] a) L. Long, S. Wang, M. Xiao, Y. Meng, *Journal of Materials Chemistry A* **2016**, 4, 10038; b) P. Yao, H. Yu, Z. Ding, Y. Liu, J. Lu, M. Lavorgna, J. Wu, X. Liu, *Frontiers in Chemistry* **2019**, 7; c) H. Zhang, M. Armand, *Israel Journal of Chemistry* **2021**, 61, 94; d) X. Zhang, J.-C. Daigle, K. Zaghib, *Materials* **2020**, 13, 2488; e) Q. Zhao, *Joule* **2019**, 3, 1569; f) F. Zheng, M. Kotobuki, S. Song, M. O. Lai, L. Lu, *Journal of Power Sources* **2018**, 389, 198; g) Y. Zheng, Y. Yao, J. Ou, M. Li, D. Luo, H. Dou, Z. Li, K. Amine, A. Yu, Z. Chen, *Chemical Society Reviews* **2020**, 49, 8790.

[16] J. Motavalli, *Nature* **2015**, 526, S96.

[17] a) J. Qiu, X. Liu, R. Chen, Q. Li, Y. Wang, P. Chen, L. Gan, S.-J. Lee,

D. Nordlund, Y. Liu, X. Yu, X. Bai, H. Li, L. Chen, *Advanced Functional Materials* **2020**, 30, 1909392; b) Z. Li, H. Zhang, X. Sun, Y. Yang, *ACS Energy Letters* **2020**, 5, 3244.

[18] K. Xu, *Chemical Reviews* **2004**, 104, 4303.

[19] Z. Zhang, J. Yang, W. Huang, H. Wang, W. Zhou, Y. Li, Y. Li, J. Xu, W. Huang, W. Chiu, Y. Cui, *Matter* **2021**, 4, 302.

[20] Y. Zhang, Y. Shi, X.-C. Hu, W.-P. Wang, R. Wen, S. Xin, Y.-G. Guo, *Advanced Energy Materials* **2020**, 10, 1903325.

[21] S. S. Hwang, C. G. Cho, H. Kim, *Electrochemistry Communications* **2010**, 12, 916.

[22] S. Choudhury, S. Stalin, D. Vu, A. Warren, Y. Deng, P. Biswal, L. A. Archer, *Nature Communications* **2019**, 10, 4398.

[23] H. Wu, Y. Xu, X. Ren, B. Liu, M. H. Engelhard, M. S. Ding, P. Z. El-Khoury, L. Zhang, Q. Li, K. Xu, C. Wang, J.-G. Zhang, W. Xu, *Advanced Energy Materials* **2019**, 9, 1902108.

[24] a) D. Brouillette, D. E. Irish, N. J. Taylor, G. Perron, M. Odziemkowski, J. E. Desnoyers, *Physical Chemistry Chemical Physics* **2002**, 4, 6063; b) P. Zeng, Y. Han, X. Duan, G. Jia, L. Huang, Y. Chen, *Materials Research Bulletin* **2017**, 95, 61.

[25] Y. Li, G. M. Veith, K. L. Browning, J. Chen, D. K. Hensley, M. P. Paranthaman, S. Dai, X.-G. Sun, *Nano Energy* **2017**, 40, 9.

[26] B. Flamme, J. Światowska, M. Haddad, P. Phansavath, V.

Ratovelomanana-Vidal, A. Chagnes, *Journal of The Electrochemical Society* **2020**, 167, 070508.

[27] a) G. Pagès, V. Gilard, R. Martino, M. Malet-Martino, *Analyst* **2017**, 142, 3771; b) K. Yoshida, M. Tsuchiya, N. Tachikawa, K. Dokko, M. Watanabe, *The Journal of Physical Chemistry C* **2011**, 115, 18384.

[28] a) D. Gyabeng, P.-A. Martin, U. Pal, M. Deschamps, M. Forsyth, L. A. O'Dell, *Frontiers in Chemistry* **2019**, 7; b) X. Bi, X. Ren, Z. Huang, M. Yu, E. Kreidler, Y. Wu, *Chemical Communications* **2015**, 51, 7665.

[29] C.-C. Su, M. He, J. Shi, R. Amine, Z. Yu, L. Cheng, J. Guo, K. Amine, *Energy & Environmental Science* **2021**, 14, 3029.

[30] J. Liu, Z. Bao, Y. Cui, E. J. Dufek, J. B. Goodenough, P. Khalifah, Q. Li, B. Y. Liaw, P. Liu, A. Manthiram, *Nature Energy* **2019**, 4, 180.

[31] A. A. Rulev, Y. O. Kondratyeva, L. V. Yashina, D. M. Itkis, *The Journal of Physical Chemistry Letters* **2020**, 11, 10511.

6. 국 문 초 록

기후 변화에 대한 우려와 에너지 공급에 대한 매우 까다로운 요구가 동시에 등장함에 따라 전기 에너지를 저장하기위한 고밀도 배터리의 개발이 시급한 기술 문제로 대두되었다. 흑연과 $LiCoO_2$를 사용하는 이온 삽입/탈리 메커니즘이 적용된 기존의 리튬 이온 배터리는 최근 EV 시장의 폭발적 확장으로부터 촉발된 매우 까다로운 에너지 요구 수준에 대해 한계에 직면했다. 따라서, 전 세계 배터리 연구자들이 다양한 차세대 리튬 이온 배터리 개발에 도전하고 있다. 그중 리튬 금속 배터리는 리튬 금속이 상용 흑연 음극(370mAh g^{-1})에 비해 훨씬 높은 비용량 (3860mAh g^{-1})을 제공하기 때문에 큰 관심을 받고 있다. 높은 이론용량으로 인해 리튬 금속은 차세대 목표 에너지 밀도 (500Wh/kg)를 달성 할 것으로 기대된다. 그러나 Li 금속의 높은 환원성으로 인해 제어되지 않은 계면 반응은 Li 금속의 수지상 성장을 초래하고 결과적으로 단락에 의한 안전 위험, 에너지 밀도 저하 및 셀 임피던스 증가와 같은 다양한 문제를 발생시킨다. 이에 대응하기 위해 다양한 전략적 접근 방식이 개발되었으며 리튬 금속 배터리가 일정 수준까지 개선되는 데 기여하였다. 덕분에 Li 금속 폴리머 배터리는 프랑스 자동차 회사인 Bolloré 에 의해 전기 자동차용으로 상용화까지

되기에 이르렀다. 그러나 성능은 여전히 진정한 의미의 '차세대 리튬 이온'이 되기에는 목표 에너지 밀도보다 훨씬 적었으며 여전히 극복해야 할 한계가 있었다.

본 연구에서는 기존에 상용화된 리튬 메탈 폴리머 배터리의 심각한 한계를 바탕으로 고전압 리튬 메탈 폴리머 배터리를 개발하기 위해 체계적인 설계 원리를 구축하고 종합적으로 적용하였다. 1) 고체 고분자 전해질의 낮은 이온 전도도를 해결하기 위해 액체 용매(1,2-dimethoxyethane)를 전해질에 포함시켰다. 단, 전해질의 리튬 금속과 호환성을 유지하기 위해 Bolloré 배터리에서와 마찬가지로 에테르 기반 폴리머 및 액체 용매를 사용하였다. 2) 에테르 기반 구성 요소의 낮은 양극 안정성을 보완하기 위해 리튬염을 농축(~3.1M)하고 가교된 고분자 매트릭스를 사용하여 용매 분자가 반응성 높은 양극 표면으로의 확산을 억제하여 결과적으로 강력하고 무기성분이 풍부한 형태의 CEI 를 형성합니다. 이는 양극에서 지속 가능한 계면 안정성을 위한 CEI 층을 형성하는 것을 의미한다.

총 세 가지의 실험군이 설정되어 비교 연구되었다. 리튬염을 DME 에 녹인 전해질, DME 와 PEO 고분자에 녹인 전해질, DME 와

가교된 고분자를 포함한 전해질이다. 각 전해질은 액체 전해질, 선형 고분자 사슬을 가진 젤 폴리머 전해질 및 가교 된 젤 폴리머 전해질을 나타낸다. 가교된 젤 폴리머 전해질을 제조하기 위해 에테르 계열 단량체, 트리에틸렌 글리콜 다이 비닐 에테르(TEGDVE)를 사용하여 양이온 개시제 리튬 다이플루오로-옥살라토보레이트 (LiDFOB) 염에 의해 중합시켰다. 가교된 고분자 매트릭스에서 용매 분자의 확산이 억제된다는 가설을 입증하기 위해 액체 및 젤 폴리머 전해질에 대해 펄스필드구배 핵자기공명 (PFG-NMR) 분광 분석을 수행하여 각 전해질에서 용매의 확산 거동을 평가하였다. 예상대로, 액체 및 선형 사슬 젤 고분자 전해질에 비해 가교된 고분자 매트릭스에서 용매 분자의 확산이 크게 억제되었다. 또한, 용매 분자뿐만 아니라 선형 고분자 사슬도 해당 젤 전해질에서 확산되는 것으로 나타났으며, 이는 가교된 젤 전해질에서 고분자 확산이 일어나지 않는 것과 대조적이다.

용매 분자의 확산과 전기 화학적 성능 간의 상관 관계를 확인하기 위해 각 전해질을 이용하여 Li|NCM 완전셀에 대해 충/방전 실험을 수행하였다. 염 농도에 관계없이 완전셀의 수명 안정성은 가교된 젤 전해질에서 가장 높았다. 완전셀 충/방전 테스트 후 양극과 음극, 각각의 분석을 통해 전해질에 따라 서로 다른 계면 현상이

유도되었다는 것을 확인할 수 있었다. 가교된 젤 전해질에서 용매 분자의 확산을 억제하기 때문에 CEI 층을 형성하는데 음이온이 주로 기여한다. Li 금속 음극 측에서는 가교된 겔 전해질에 의해 기계적으로 억제된 수지상 성장이 전기화학적 성능에 기여한다. 종합적으로, 본 연구에서 구성하고 활용한 설계 원리가 다양한 분광 및 계면 분석에서 입증된 바와 같이 목적했던 대로 작동한다는 것을 확인할 수 있었다.